# CREATION OF MOLECULAR GLASSES – SYNTHESIS, PROPERTIES, AND APPLICATION

1997

HIROSHI KAGEYAMA
OSAKA UNIVERSITY

# CREATION OF MOLECULAR GLASSES – SYNTHESIS, PROPERTIES, AND APPLICATION

(分子性ガラスの創製－合成、物性および応用)

1997

HIROSHI KAGEYAMA
OSAKA UNIVERSITY

# CONTENTS

# INTRODUCTION

Glasses appeared in the history of the mankind as early as at the Mesopotamian age more than 4000 years ago and used as materials for arts, crafts, building, and so on. However, the essential nature of glasses were not fully understood.

Research on glasses or amorphous solids has become one of the interesting subjects in the field of materials science, because (i) glasses constitute a novel class of materials, (ii) the preparation techniques of the amorphous glass have been progressed, and (iii) the glasses are expected to be a promising materials for devices.

The term *glass* is used to describe the special group of noncrystalline solids that can be prepared by the quenching the melt and distinguished from the term *amorphous solid.* The term *amorphous solid* is the classification from the structural view point. The essential nature of *glass* is that it is in a "thermodynamically nonequilibrium state" in contrast to *amorphous solids* which have " disordered" structures in the absence of long-range order. The order of atoms or molecules can be characterized by X-ray diffraction (XRD). The XRD patterns of crystal show sharp peaks characteristic of the periodically ordered structure of crystal. On the other hand, the XRD patterns of amorphous solids show only broad halos characteristic of the disordered structure. Figure I shows temperature dependence of the volume of a pure material. When the crystal, which is in a thermodynamically equilibrium state (line AB), is heated, the first-order phase transition (melt) takes place at the temperature B, leading to isotropic liquid (line CD). When the isotropic liquid is quenched without crystallization (C $\rightarrow$ E), the resulting state of the material is a supercooled liquid (thermodynamically quasi-equilibrium state), and the volume abruptly contracts. The viscosity also drastically increases with decreasing temperature and reaches *ca.* $10^{13}$ Poise at the temperature E. The state cannot be reached the equilibrium at the temperature E, and the atomic or molecular motions freeze (E $\rightarrow$ G). The temperature E, which changes depending on its thermal history, is defined as the glass-transition temperature ($T_g$). The state below the $T_g$ is the nonequilibrium "glassy

state". The other nonequilibrium systems such as the crystal with defects is also in "glassy state" from the thermodynamical view point.

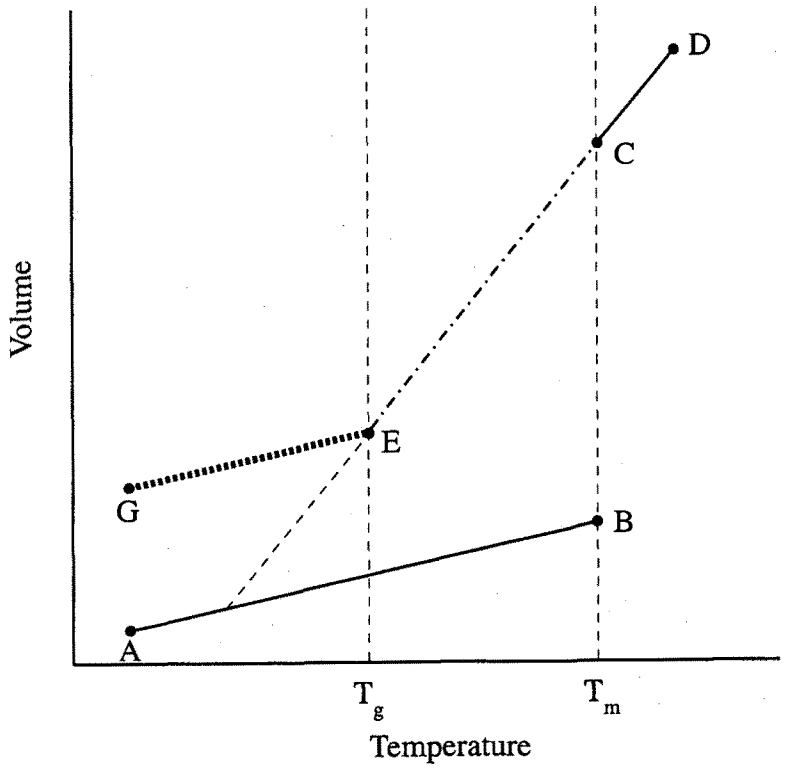


**Figure I** Temperature dependencies of volume of a pure material. AB: Crystal; CD: Liquid; CE: supercooled liquid; GE: Glass.

The amorphous glassy state is generally prepared by the following two processes; (1) a process of supplying very high energy into the original system in order to obtain the disordered structure and (2) a process of taking its kinetic energy from the system very rapidly in order to freeze the motion. The latter procedure is called the quenching. The quench rate required to make an amorphous state different depending on the material. In principle, *any* material can be transformed into an amorphous glassy state when the quench rate is sufficiently rapid to make the amorphous glassy state.

Amorphous materials have recently attracted attention as a novel class of functional materials with excellent processability, transparency, isotropic properties, and homogeneous properties owing to the absence of grain boundaries. With regard to amorphous organic materials, polymers and composite polymer systems, where low

molecular-weight functional organic materials are dispersed in polymer binders, are known. Although amorphous or quasi-amorphous films of certain organic compounds, *e.g.*, biphenyl, terphenyl, and polycyclic aromatic hydrocarbons such as quaterrylene, naphthacene, and violanthrene, can be formed by vacuum deposition at very low temperatures,[1-8] little attention was paid to low molecular-weight organic compounds that form stable amorphous glasses above room temperature, since low molecular-weight organic compounds generally tend to crystallize readily. Only a few scattered examples of organic compounds that form amorphous glasses above room temperature were known.[9-11]

Creation of low molecular-weight organic compounds that readily form stable amorphous glasses with relatively high glass-transition temperatures, namely "molecular glasses" are of interest and significance, because they are expected to constitute a novel class of organic materials and studies on molecular glasses open up a new field in organic materials science that deals with the correlation between molecular structure and glass-forming properties, the relaxation processes of molecular glasses, investigation of intrinsic properties of the molecular glass, dynamic control of properties and functions of molecular glasses using their morphological changes, and application of molecular glasses as functional materials for optoelectronic and electronic devices.

In our laboratory, several novel families of organic π-electron systems, which we have referred to as "starburst" molecules in view of their molecular structures, have been designed and synthesized for making molecular glasses with photo- and electro-activities.[12-24] They include 4,4',4"-tris(diphenylamino)triphenylamine (TDATA) and its derivatives[12-14] including 4,4',4"-tri(*N*-carbazolyl)triphenylamine,[15] 4,4',4"-tris-(1-naphthylphenylamino)triphenylamine and 4,4',4"-tris(2-naphthylphenylamino)-triphenylamine,[16] 1,3,5-tris(diphenylamino)benzene (TDAB) and its derivatives[17-20] including 1,3,5-tris[*N*-(4-diphenylaminophenyl)phenylamino]benzene,[21] 1,3,5-tris-[4-(diphenylamino)phenyl]benzene (TDAPB) and its derivatives.[22] In addition, as a part of studies of molecular glasses in our laboratory, novel low molecular-weight organic compounds such as tri(biphenyl-4-yl)amine, and tri(*p*-terphenyl-4-yl)amine,[25] and

arylaldehyde and arylketone hydrazones[27–30] have also been studied. They have been found to readily form amorphous glasses with well-defined glass-transition temperatures above room temperatures except for TDAB. A few guidelines for molecular design of molecular glasses, namely, nonplanar molecular structure and the presence of different conformers, have been shown. Furthermore, we have found that the introduction of a rigid moiety into nonplanar molecules leads to an increase in the glass-transition temperature. In addition, we have been studying the intrinsic properties and application of molecular glasses. Some of them have been found to function as charge transport materials[26–30] and as excellent materials for use in organic electroluminescent devices.[15,16,23–31]

This thesis is concerned with the molecular design and synthesis of novel classes of low molecular-weight organic compounds, elucidation of their charge transport properties, and application as functional materials such as resist materials for lighography. The thesis consists of four chapters. In chapter 1, the design and synthesis of a novel molecular glass, tris[4-(2-thienyl)phenyl]amine, and its structures and morphology are described. In chapter 2, the design and synthesis of a novel family of starburst molecules, halogen substituted 1,3,5-tris(diphenylamino)benzenes, and their glass-forming properties are described and the effect of halogen substituent on the ease of glass formation, stability of the glassy state and the glass-transition temperature is discussed. In chapter 3, charge transport in the molecular glass is investigated and the correlation between molecular structure and charge-transport properties is discussed. Chapter 4 deals with an application of molecular glasses as functional materials. A new concept of "molecular resist" is proposed and a novel class of low molecular-weight organic resist materials based on this concept is created.

# CHAPTER 1

## Creation of a Molecular Glass – Synthesis, Structure, and Morphology of Tris[4-(2-thienyl)phenyl]amine

### 1-1 Introduction

We have reported that several novel families of organic π-electron systems, which we refer to as "starburst" molecules in view of their molecular structures, form amorphous glasses when cooled from the melts. We have also investigated the glass-forming property of π-electron organic compounds containing simpler structures than those of starburst molecules, and found that whereas triphenylamine does not form an amorphous glass even when the melt sample is rapidly cooled with liquid nitrogen, tri(biphenyl-4-yl)amine (TBA) can form an amorphous glass when cooled from the melt,[25,26] although the glassy state of TBA is much less stable than those of starburst molecules.

This chapter deals with the design, synthesis, structure, and morphology of a new molecular glass, tris[4-(2-thienyl)phenyl]amine (TTPA) containing three thienyl groups as a replacement for the three phenyl groups in TBA. Whereas triphenylamine instantly crystallizes even when the melt sample is rapidly cooled with liquid nitrogen, TTPA is found to readily form an amorphous glass. The morphological changes, molecular and crystal structures of TTPA are investigated. The results are compared with those of previously reported tri(biphenyl-4-yl)amine and the effect of number of conformers on the glass-forming properties is discussed.

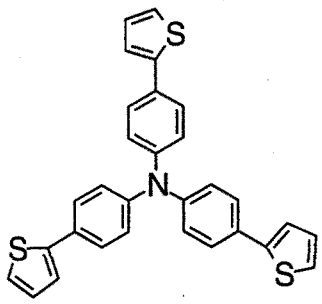


TTPA

## 1-2 Experimental

Preparation of TTPA

A solution of 2-thienylmagnesium bromide, prepared by refluxing a solution of 2-bromothiophene (7.85 g, 48.12 mmol) in 10 ml ether in the presence of magnesium turnings (1.17 g, 48.12 mmol), was added to a solution of tris(4-iodophenyl)amine (5.0 g, 8.02 mmol) in 25 ml THF in the presence of $Ni(dppp)Cl_2$ (42 mg, 0.077 mmol) as a catalyst under nitrogen atmosphere. After the solution was refluxed for 20 h, diluted hydrochloric acid was added to the resulting pale yellow solution at 0 ℃ to quench the reaction. The solution was extracted with benzene, washed with water, and then dried over sodium sulfate. After removing the solvent, the residue was chromatographed on a silica-gel column using a mixed solvent of benzene and hexane (1:4) as an eluent, followed by recrystallization from hexane to give TTPA as yellow needles (1.35 g, 34.2 %). MS m/z 491 ($M^+$). Calcd. for C30H21NS3: C, 73.61; H, 4.34; N, 2.85%, Found: C, 73.32; H, 4.28; N, 2.85%. $^1H$ NMR (400 MHz; solvent: dioxane-$d_8$; standard:tetramethylsilane) $\delta$=7.05 (dd, 3H), 7.15 (d, 6H), 7.30 (m, 6H), 7.53 (d, 6H).

Measurements

Cyclic voltammetry was carried out for a dichloromethane solution containing TTPA ($1.0 \times 10^{-3}$ mol $dm^{-3}$) and tetrabutylammonium perchlorate (0.1 mol $dm^{-3}$), by using platinum plates as the working and counter electrodes and $Ag/AgNO_3$ (0.01 mol $dm^{-3}$ in acetonitrile) as the reference electrode.

Morphological changes were examined by differential scanning calorimetry (DSC), X-ray diffraction (XRD), and polarizing microscopy.

X-Ray Crystal Structure Analysis of TTPA

Since a good quality single crystal of TTPA for X-ray crystal structure analysis could not be obtained by recrystallization from hexane, a single crystal was grown from a benzene solution to give a prism with dimensions of approximately 0.15 x 0.23 x 0.38 $mm^3$, which contains the solvent molecule benzene. The crystal data were as follows: $C30H21NS3(C_6H_6)_{0.5}$, M=530.74, monoclinic, space group $P2_1/c$, a=13.311(4), b=17.869(5), c=11.662(5) Å, β=101.71(3)°, V=2716(2) $Å^3$, Z=4, Dc=1.30 $gcm^{-1}$, μ(Mo Kα)=3.01 $cm^{-1}$.

X-Ray diffraction data were collected by the ω-2θ scan technique up to 2θ=55° on Rigaku AFC-5R automatic four-circle diffractometer using graphite monochromatized Mo Kα radiation (λ=0.7107 Å). No significant intensity decay of three standard reflections was detected as measured after every 150 reflections. Of the 6752 reflections measured, 1946 reflections were observed ($|F_o| > 3\sigma(F_o)$). The intensity data were corrected for the Lorentz and polarization effects, but not for absorption.

The structure was solved by a direct method (SAPI91)[32] and expanded using Fourier technique (DIRDIF).[33] The structure was refined anisotropically for all the non-hydrogen atoms by a full-matrix least-squares method. During the refinement process, two thienyl groups (T2 and T3) of the TTPA molecule were found to be disordered; each takes two positions differing about 180° around the C-C single bond connecting the thienyl group and the phenyl group. Thus, the structure refinement was carried out under the following conditions. (i) The positional parameters and temperature factors of C20, C23, C31, and C34 were assumed to be equal to those of S20, S23, S31, and S34, respectively. (ii) The site occupancy factors (sof) of S20, S23, S31, S34, C20, C23, C31, and C34 were refined under the following conditions;

$$sof(S20) = 1 - sof(S23) = 1 - sof(C20) = sof(C23)$$

$$sof(S31) = 1 - sof(S34) = 1 - sof(C31) = sof(C34)$$

(iii) The hydrogen atoms in the disordered thienyl groups and the solvent benzene molecule were omitted from the calculation and the other hydrogen atoms were located at their calculated positions. Their isotropic temperature factors were assumed to be equal to the equivalent temperature factors of the carbon atoms bonded.

The function minimized was $\Sigma w(|F_o|-|F_c|)^2$, where the weighting function was $w=1/\sigma^2(F_o)$. The atomic scattering factors were taken from those of the International Tables for X-Ray Crystallography.[34] The R and Rw values at the last stage were 0.088 and 0.059, respectively. All calculations were performed using the TEXSAN crystallographic software package of Molecular Structure Computation[35] by a workstation (INDIGO R4000, Silicon Graphics) at the Department of Applied Chemistry, Faculty of Engineering, Osaka University. The atomic coordinates of the non-hydrogen atoms with the equivalent temperature factors[36] are given in Table 1-1.

**Table 1-1** Positional parameters, equivalent temperature factors, and site occupancy factors (sof) for non-hydrogen atoms of $TTPA(C_6H_6)_{0.5}$.

| atom | x | y | z | B(eq) | sof |
|---|---|---|---|---|---|
| S(9) | -0.4938(3) | -0.6885(2) | -0.6278(3) | 9.3(1) | |
| S(20) | -0.0482(3) | -0.7443(3) | 0.2791(4) | 6.6(2) | 0.585 |
| S(23) | -0.0180(4) | -0.6127(4) | 0.3879(6) | 8.2(2) | 0.415 |
| S(31) | -0.2960(6) | -0.1350(4) | -0.0665(7) | 7.1(3) | 0.251 |
| S(34) | -0.2076(3) | -0.1264(2) | -0.2464(3) | 5.5(1) | 0.749 |
| N(1) | -0.2325(7) | -0.4996(5) | -0.1593(8) | 5.3(3) | |
| C(2) | -0.266(1) | -0.5402(6) | -0.2666(9) | 4.3(3) | |
| C(3) | -0.3685(9) | -0.5355(6) | -0.324(1) | 4.9(3) | |
| C(4) | -0.4025(8) | -0.5767(6) | -0.424(1) | 4.6(3) | |
| C(5) | -0.3346(8) | -0.6212(6) | -0.4695(8) | 3.5(3) | |
| C(6) | -0.2327(8) | -0.6239(6) | -0.411(1) | 4.2(3) | |
| C(7) | -0.1981(8) | -0.5837(6) | -0.310(1) | 4.7(3) | |
| C(8) | -0.3695(7) | -0.6655(6) | -0.5772(9) | 3.9(3) | |
| C(10) | -0.466(1) | -0.7390(8) | -0.742(1) | 7.8(4) | |
| C(11) | -0.368(1) | -0.7377(8) | -0.742(1) | 6.9(4) | |
| C(12) | -0.3099(8) | -0.6948(6) | -0.650(1) | 5.1(3) | |
| C(13) | -0.1894(9) | -0.5377(7) | -0.057(1) | 4.5(3) | |
| C(14) | -0.2147(8) | -0.6109(7) | -0.036(1) | 5.1(3) | |
| C(15) | -0.1712(9) | -0.6480(6) | 0.067(1) | 5.1(4) | |
| C(16) | -0.0998(8) | -0.6138(7) | 0.157(1) | 4.8(4) | |
| C(17) | -0.0739(8) | -0.5413(7) | 0.135(1) | 5.2(3) | |
| C(18) | -0.1165(9) | -0.5038(6) | 0.033(1) | 5.0(3) | |
| C(19) | -0.0574(7) | -0.6544(8) | 0.268(1) | 5.4(4) | |
| C(20) | -0.0482 | -0.7443 | 0.2791 | 6.6 | 0.415 |
| C(21) | 0.000(1) | -0.750(1) | 0.417(2) | 9.4(6) | |
| C(22) | 0.015(1) | -0.681(1) | 0.468(1) | 9.0(5) | |
| C(23) | -0.0180 | -0.6127 | 0.3879 | 8.2 | 0.585 |
| C(24) | -0.2404(9) | -0.4219(6) | -0.159(1) | 4.5(3) | |
| C(25) | -0.2798(9) | -0.3836(7) | -0.074(1) | 5.1(4) | |
| C(26) | -0.2851(8) | -0.3055(6) | -0.0749(9) | 4.6(3) | |
| C(27) | -0.2537(7) | -0.2612(6) | -0.1590(9) | 3.8(3) | |
| C(28) | -0.2182(8) | -0.3029(6) | -0.2470(9) | 4.8(3) | |
| C(29) | -0.2132(9) | -0.3802(7) | -0.247(1) | 5.1(3) | |
| C(30) | -0.2567(7) | -0.1805(5) | -0.153(1) | 3.9(3) | |
| C(31) | -0.2960 | -0.1350 | -0.0665 | 7.1 | 0.749 |
| C(32) | -0.279(1) | -0.0552(7) | -0.093(1) | 7.7(5) | |
| C(33) | -0.233(1) | -0.0448(6) | -0.187(1) | 6.4(4) | |
| C(34) | -0.2076 | -0.1264 | -0.2464 | 5.5 | 0.251 |
| C(35) | -0.475(2) | -0.043(2) | -0.397(3) | 10.6(9) | |
| C(36) | -0.529(2) | -0.077(1) | -0.501(5) | 10.7(7) | |
| C(37) | -0.554(2) | -0.032(3) | -0.603(2) | 10.5(8) | |

Apparatus

Electronic absorption and fluorescence spectra were taken on a Hitachi U-3200 spectrophotometer and a Hitachi 850 fluorescence spectrophotometer, respectively. DSC measurement was made using a Seiko DSC220C. X-Ray diffraction measurement was carried out with a M18XHF-SRA X-ray diffractometer (MAC Science). Polarizing microscopy was performed with an Optiphot X2 (Nikon) microscope, fitted with a TH-600PM hot stage (Linkam) and crossed polarizers. Cyclic voltammetry was carried out with a Hokuto Denko HA-501 Potentiostat and a HB-104 Function Generator.

## 1-3 Synthesis and Molecular Properties

Tris[4-(2-thienyl)phenyl]amine was successfully synthesized by the Grignard reaction of tris(4-iodophenyl)amine with 2-bromothiophene in THF (Scheme 1.1).

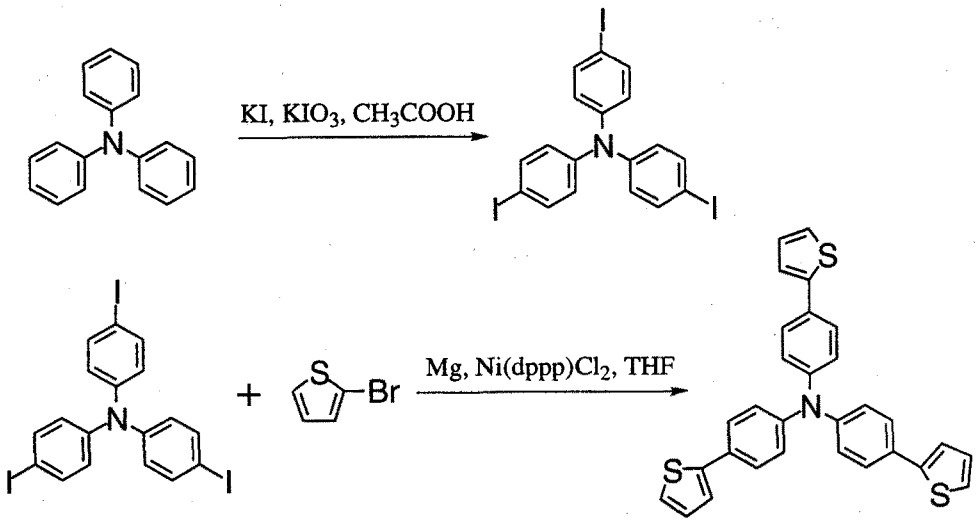


**Scheme 1.1** Synthesis of TTPA

TTPA shows an electronic absorption band with $\lambda_{max}$ at 363 nm (log $\varepsilon$ = 4.8) and a fluorescence band with $\lambda_{max}$ at 422 nm. The fluorescence quantum yield of TTPA in a THF solution was determined to be 0.68.

TTPA shows a reversible anodic oxidation process, as characterized by cyclic voltammetry. The half-wave oxidation potential of TTPA ($E^{ox}_{1/2}$) in dichloromethane was determined to be 0.57 V *vs.* $Ag/Ag^+$ (0.01 mol $dm^{-3}$). The second oxidation process of TTPA was irreversible.

## 1-4 Glass Formation and Polymorphism

It was found that TTPA readily forms an amorphous glass when the melt sample was cooled either rapidly with liquid nitrogen or slowly on standing in air. In addition to the formation of a glass, TTPA was found to exhibit polymorphism. Figure 1-1 shows DSC curves of TTPA. When a crystalline sample of TTPA (crystal A) obtained

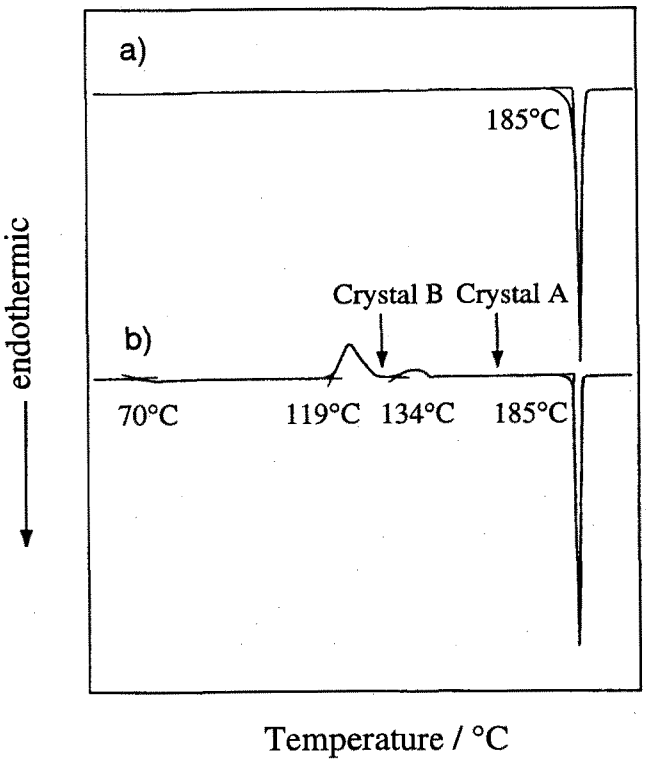


**Figure 1-1** DSC curves of TTPA. Heating rate : 1 °Cmin$^{-1}$. a) Crystalline sample (Crystal A) obtained by recrystallization from hexane. b) Glass sample obtained by cooling the melt.

by recrystallization from hexane was heated, an endothermic peak due to melting was observed at 185 ℃. When the melt sample was cooled down either rapidly with liquid nitrogen or slowly on standing in air, it formed an amorphous glass *via* a supercooled liquid state. When the glass sample was heated, glass transition took place at 70 ℃. On heating above the $T_g$, crystallization occurred at 119 ℃ to form another crystal (crystal B). On further heating, an exothermic peak due to solid-solid phase transformation from the crystal B to the crystal A was observed at 134 ℃, followed by the melting of the crystal A at 185 ℃. The same trace was observed over many cycles.

The formation of the glass and the crystals A and B was evidenced by X-ray diffraction (Figure 1-2). The crystalline sample formed by heating the glass to *ca.* 160 ℃ exhibits the same sharp diffraction peaks as those of the crystal A obtained by recrystallization from hexane. The crystalline sample formed by heating the glass to *ca.* 130 ℃ exhibits new peaks which are not observed for the crystal A. This indicates the formation of a different crystal form (crystal B) at this temperature, which undergoes the

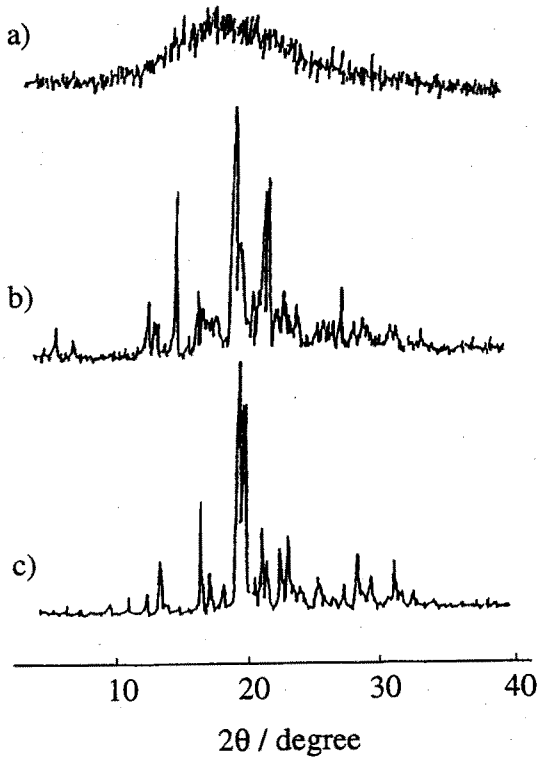


**Figure 1-2** X-Ray diffraction patterns of TTPA for a) the glass sample obtained by cooling the melt, and the crystalline samples obtained by heating the glass to b) *ca.* 130 ℃, and c) *ca.* 160 ℃.

solid-solid phase transformation from the crystal B to the crystal A on heating, as evidenced from the DSC curve. On the other hand, the glass obtained by cooling the melt sample exhibited only a broad halo. The morphological changes of TTPA are summarized in Scheme 1.2.

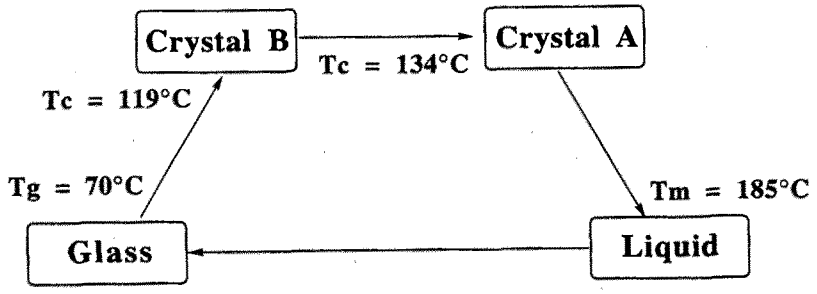


**Scheme 1.2** Morphological Changes of TTPA

## 1-5 X-Ray Structure Analysis

Molecular and Crystal Structures

Determination of molecular and crystal structures is expected to provide information on the relationship between molecular structure and glass-forming properties. The TTPA crystal submitted to X-ray crystal structure analysis was grown from a benzene solution, which contained the solvent molecule benzene in a molar ratio of TTPA:$C_6H_6$ = 2:1. The atomic coordinates of non-hydrogen atoms with equivalent temperature factors and site occupancy factors (sof) are listed in Table 1-1.

Figure 1-3 shows the molecular structure of TTPA in the crystal of TTPA$(C_6H_6)_{0.5}$, where the three phenyl and thienyl rings in TTPA are referred to as P1, P2, and P3, and T1, T2, and T3, respectively. The central triphenylamine moiety has a propeller-like structure. That is, the dihedral angles between the plane consisting of the three carbon atoms bonded to the nitrogen atom and the least square planes of the phenyl rings P1, P2, and P3 are 59.7, 27.8, and 45.9°, respectively. The nitrogen atom deviates from the

plane consisting of the three carbon atoms bonded to the nitrogen atom and the distance between the plane and the nitrogen atom is 0.01 Å. In addition, the thienyl groups are twisted against the phenyl groups bonded. When viewed from the nitrogen atom in Figure 3, the thienyl ring T2 is twisted clockwise by 26.4° against the inside phenyl ring P2, while the thienyl rings T1 and T3 are twisted counterclockwise by 20.2 and 6.5°, respectively, against the corresponding inside phenyl rings P1 and P3. The two thienyl groups, T2 and T3, were found to be disordered; each takes two positions differing about 180° around the C-C single bond connecting the thienyl group and the phenyl group. The population ratios of the disordered thienyl groups T2 and T3 were estimated from the values of site occupancy factors (sof) of sulfur atoms; sof(S20):sof(S23) and sof(S31):sof(S34) were 0.59:0.41 and 0.25:0.75, respectively. There are four TTPA and two benzene molecules in a unit cell without any significant short intermolecular contact. Figure 1-4 shows the crystal structure of TTPA$(C_6H_6)_{0.5}$.

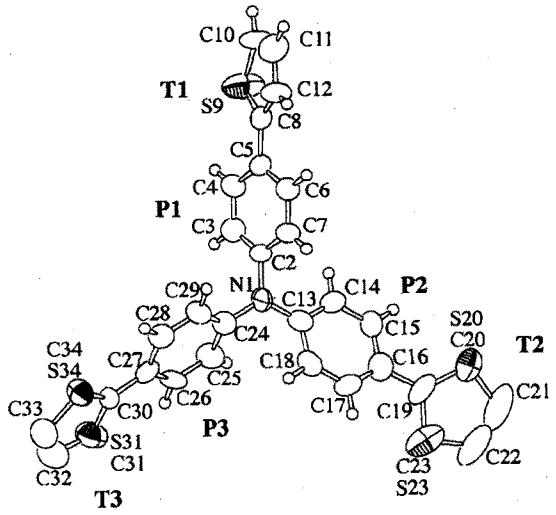


**Figure 1-3** Molecular Structure of TTPA.

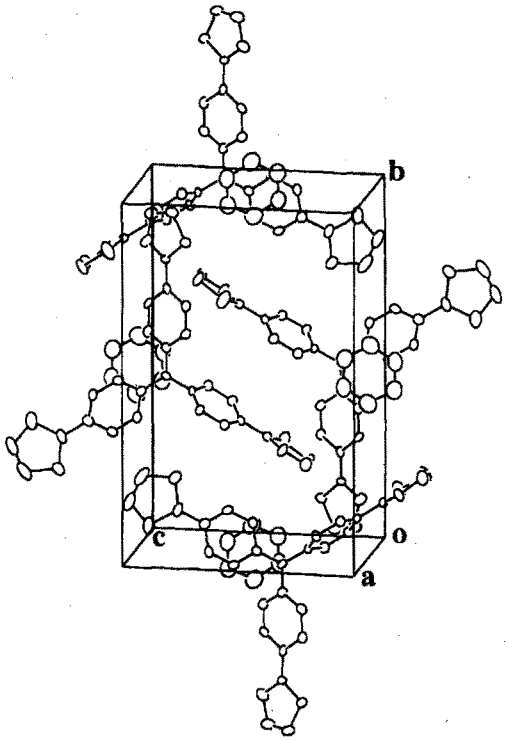


**Figure 1-4** Crystal structure of TTPA$(C_6H_6)_{0.5}$.

## 1-6 Discussion

In the present study, TTPA was found to form an amorphous glass with a well-defined, relatively high Tg of 70 ℃. The results of X-ray crystal structure analysis for a TTPA crystal show that TTPA has a nonplanar structure. It is thought that the nonplanar molecular structure plays an important role in the formation of a glass. That is, the nonplanar molecular structure prevents the ready packing of molecules to form a crystal. In addition, the existence of different conformers is suggested to facilitate the formation of the glass as discussed below.

As compared with tri(biphenyl-4-yl)amine,[26] TTPA forms an amorphous glass more readily. That is, whereas tri(biphenyl-4-yl)amine requires rapid cooling of the melt sample at a cooling rate faster than *ca.* 30 ℃ $min^{-1}$ to form an amorphous glass, TTPA forms a glass even when the melt sample is cooled at a cooling rate as slow as 1 ℃ $min^{-1}$. This result shows that the replacement of the phenyl groups in tri(biphenyl-4-yl)amine by the three thienyl groups makes glass formation easier. We have previously reported that whereas 1,3,5-tris(diphenylamino)benzene (TDAB) readily crystallizes even when the

melt is rapidly cooled with liquid nitrogen, 1,3,5-tris(phenyl-2-thienylamino)benzene (α-TPTAB) and 1,3,5-tris(phenyl-3-thienylamino)benzene (β-TPTAB), where the three phenyl groups in TDAB are replaced by the thienyl group, form amorphous glasses.[20] It is suggested that the replacement of the three phenyl groups in tri(biphenyl-4-yl)amine and TDAB by three asymmetric aromatic thienyl groups increases the number of conformers of the molecules, facilitating glass formation. The increase in the number of conformers is supported by the result of the X-ray crystal structure analysis that the TTPA, α-TPTAB, and β-TPTAB molecules have disordered structures due to the thienyl group. Such disordered structures have also been reported for other compounds containing the thienyl group.[37–39]

It is shown that the TTPA glass, which is in the thermodynamically nonequilibrium state, is transformed into a thermodynamically equilibrium, metastable supercooled liquid at $T_g$, finally producing the crystal A *via* the metastable crystal B, as illustrated by the schematic free energy - temperature curves (Figure 1-5). This phenomenon of polymorphism observed for TTPA suggests that different conformers exist for TTPA. The existence of different conformers is thought to prevent the packing of the molecules, facilitating glass formation.

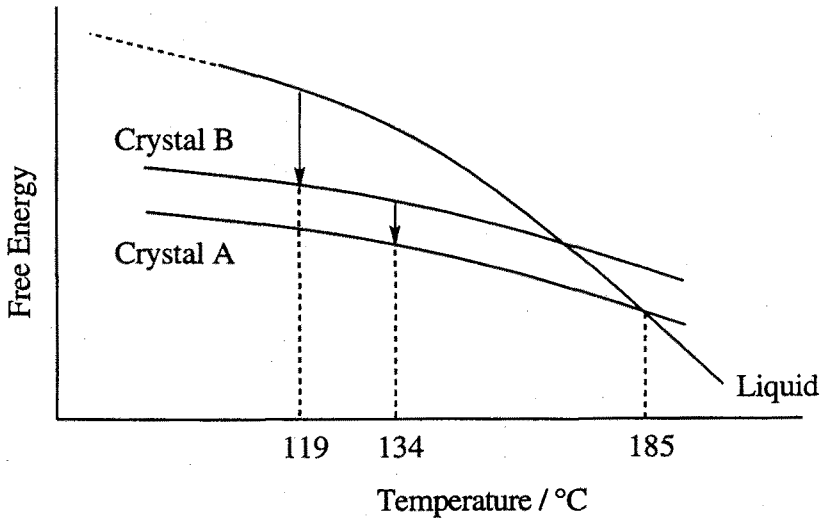


**Figure 1-5** Schematic free energy – temperature curves for TTPA.

## 1-7 Conclusion

It is found that TTPA readily forms an amorphous glass with a relatively high $T_g$ of 70 ℃, constituting a new molecular glass. As compared with TBA, TTPA forms an amorphous glass more readily. In addition to the formation of a glass, TTPA was found to exhibit polymorphism and found to have disordered structures. These results indicate that TTPA has several conformers whose conformational energies are almost the same. This is responsible for the easier glass formation of TTPA than that of TBA. That is, the increase the number of conformers by replacement of phenyl groups in TBA by thienyl groups lowers the symmetry of the molecule and prevents crystallization. This result presents a guideline for molecular design for creation of molecular glasses.

# CHAPTER 2

## Creation of Molecular Glasses – Synthesis and Glass-forming Property of a Novel Family of Starburst Molecules, Halogen Substituted 1,3,5-Tris(diphenylamino)benzenes

### 2-1 Introduction

We have already reported that whereas 1,3,5-tris(diphenylamino)benzene (TDAB) instantly crystallizes even when rapid cooled with liquid nitrogen, methyl-substituted derivatives of TDAB, *o*-, *m*-, and *p*-MTDAB readily form amorphous glasses when cooled from the melts. It was found that the methyl substituent exerts a striking effect on the formation of the glass. It is thought that incorporation of the methyl group at the *o*-, *m*-, and *p*-position of the phenyl group in TDAB increases the number of conformers of the molecules and the mode of packing of molecules, thus preventing crystallization. In order to establish the guidelines for molecular design of molecular glasses, it is important to confirm whether such substituent effect on the glass-forming property is observed for *any* substituent other than the methyl substituent or not.

We report here the design, synthesis, and glass-forming property of a novel family of halogen substituted TDABs, 1,3,5-tris(2-fluorophenylphenylamino)benzene (*o*-FTDAB), 1,3,5-tris(3-fluorophenylphenylamino)benzene (*m*-FTDAB), 1,3,5-tris-(4-fluorophenylphenylamino)benzene (*p*-FTDAB), 1,3,5-tris(2-chlorophenylphenyl-amino)benzene (*o*-ClTDAB), 1,3,5-tris(3-chlorophenylphenylamino)benzene (*m*-ClTDAB), 1,3,5-tris(4-chlorophenylphenylamino)benzene (*p*-ClTDAB), 1,3,5-tris(2-bromophenylphenylamino)benzene (*o*-BrTDAB), 1,3,5-tris(3-bromophenylphenyl-amino)benzene (*m*-BrTDAB), 1,3,5-tris(4-bromophenylphenylamino)benzene (*p*-BrTDAB). These new compounds were found to readily form amorphous glasses when cooled from the melts and the striking effect of halogen substituent on the ease of glass formation, stability of the glassy state, and glass-transition temperature was observed.

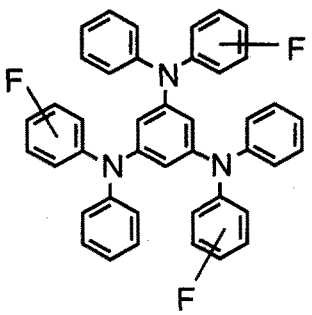

*o-*, *m-*, *p*-FTDAB

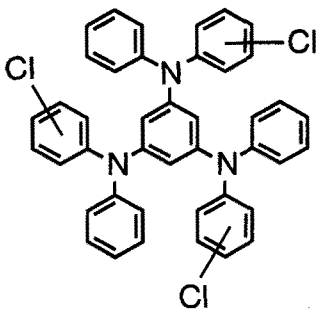

*o-*, *m-*, *p*-ClTDAB

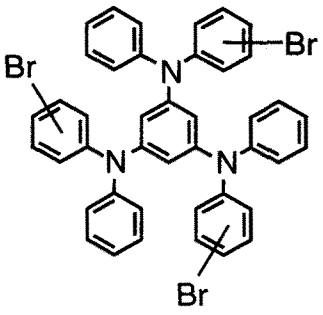

*o-*, *m-*, *p*-BrTDAB

## 2-2 Experimental

Preparation of XTDABs

*o-*, *m-*, and *p*-XTDABs(X=F, Cl, Br) were prepared by the following way : 1,3,5-tris(phenylamino)benzene, which was prepared from phloroglucinol and aniline according to the method in the literature,[40] was reacted with corresponding halogenoiodobenzene in decaline at 170℃ for 30h in the presence of copper powder and potassium hydroxide under nitrogen atmosphere. The resulting mixture was extracted with toluene. After evaporation of toluene, the residue was chromatographed on silica gel using a mixed solvent of toluene and hexane as a eluent. Recrystallization from toluene / hexane gave colorless powder. These compounds were identified by mass spectrometry, various spectroscopies, and elemental analysis. $^1$H NMR spectra were recorded at 400MHz using acetone-$d_6$ as a solvent and tetramethylsilane as a standard.

*o*-FTDAB MS: m/z 633($M^+$). Calcd. for C42H30N3F3: C,79.60 ; H,4.77 ; N,6.63 ; F,8.99%. Found: C,79.62 ; H,4.65 ; N,6.61%. $^1$H NMR (ppm): δ=6.20(3H,s), 6.91(3H,t), 6.97(6H,d), 7.08-7.17(12H,m), 7.19(6H,t). *m*-FTDAB MS: m/z 633($M^+$). Calcd. for C42H30N3F3: C,79.60 ; H,4.77 ; N,6.63 ; F,8.99%. Found: C,79.63 ; H,4.73 ; N,6.54%. $^1$H NMR (ppm): δ=6.44(3H,s), 6.67(3H,t), 6.75(3H,d), 6.84(3H,d), 7.04(3H,t), 7.11(6H,d), 7.21(3H,q), 7.27(6H,t). *p*-FTDAB MS: m/z 633($M^+$). Calcd. for C42H30N3F3: C,79.60 ; H,4.77 ; N,6.63 ; F,8.99%.

Found: C,4.67 ; H,79.53 ; N,6.53%. $^1$H NMR (ppm): δ=6.26(3H,s), 6.94(3H,t), 7.01(6H,t), 7.02(6H,d), 7.07(6H,q), 7.21(6H,t). *o*-ClTDAB MS: m/z 683($M^+$). Calcd. for C42H30N3Cl3: C,73.85 ; H,4.43 ; N,6.15 ; Cl,15.57%. Found: C,73.98 ; H,4.31 ; N,6.19 ; Cl,15.76%. $^1$H NMR (ppm): δ=6.10(3H,s), 6.88(3H,t), 6.91(6H,d), 7.15(6H,t), 7.16-7.23(6H,m), 7.28(3H,t), 7.42(3H,d). *m*-ClTDAB MS: m/z 683($M^+$). Calcd. for C42H30N3Cl3: C,73.85 ; H,4.43 ; N,6.15 ; Cl,15.57%. Found: C,73.95 ; H,4.41 ; N,6.08 ; Cl,15.63%. $^1$H NMR (ppm): δ=6.41(3H,s), 6.94(3H,d), 6.98(3H,d), 6.99(3H,s), 7.05(3H,t), 7.11(6H,d), 7.21(3H,t), 7.29(6H, t). *p*-ClTDAB MS: m/z 683($M^+$). Calcd. for C42H30N3Cl3: C,73.85 ; H,4.43 ; N,6.15 ; Cl,15.57%. Found: C,73.85 ; H,4.39 ; N,6.16 ; Cl,15.69%. $^1$H NMR (ppm): δ=6.35(3H,s), 7.00(3H,t), 7.03(6H,d), 7.07(6H,d), 7.22(6H,d), 7.25(6H,t). *o*-BrTDAB MS: m/z 817($M^+$). Calcd. for C42H30N3Br3: C,61.79 ; H,3.70 ; N,5.15 ; Br,29.36%. Found: C,61.74 ; H,3.58 ; N,5.02 ; Br,29.43%. $^1$H NMR (ppm): δ=6.09(3H,s), 6.87(3H,t), 6.91(6H,d), 7.12-7.16(9H,m), 7.19(3H,d), 7.33(3H,t), 7.61(3H,d). *m*-BrTDAB MS: m/z 817($M^+$). Calcd. for C42H30N3Br3: C,61.79 ; H,3.70 ; N,5.15 ; Br,29.36%. Found: C,61.79 ; H,3.72 ; N,5.07 ; Br,29.43%. $^1$H NMR (ppm): δ=6.40(3H,s), 7.02(3H,d), 7.05(3H,t), 7.08(3H,d), 7.11(6H,d), 7.14(3H,s), 7.17(3H,t), 7.30(6H,t). *p*-BrTDAB MS: m/z 817($M^+$). Calcd. for C42H30N3Br3: C,61.79 ; H,3.70 ; N,5.15 ; Br,29.36%. Found: C,61.74 ; H,3.61 ; N,5.13 ; Br,29.41%. $^1$H NMR (ppm): δ=6.36(3H,s), 6.98(6H,d), 7.01(3H,t), 7.07(6H,d), 7.26(6H,t), 7.36(6H,d).

Measurement

Cyclic voltammetry was carried out for a dichloromethane solution containing *o*-, *m*-, and *p*-XTDABs (1.0 x $10^{-3}$ mol $dm^{-3}$) and tetra-*n*-butylammonium perchlorate (0.1 mol $dm^{-3}$), by using platinum plates as the working and counter electrodes and $Ag/AgNO_3$ (0.01 mol $dm^{-3}$ in acetonitrile) as the reference electrode. UV-vis absorption spectrometry was performed in tetrahydrofuran solution.

Morphological changes were characterized by differential scanning calorimetry (DSC), X-ray diffraction (XRD), and polarizing microscopy.

Apparatus

Electronic absorption was taken on a Hitachi U-3200 spectrophotometer. DSC measurement was made using a Seiko DSC220C calorimeter. Cyclic voltammetry was carried out with a Hokuto Denko HA-501 Potentiostat and a HB-104 Function Generator. X-Ray diffraction was carried out with a Rotaflex RU200 (Rigaku) X-ray diffractometer. Polarizing microscopy was performed with an Optiphot X2 (Nikon) microscope, fitted with a TH-600PM hot stage (Linkam) and crossed polarizers.

## 2-3 Synthesis and Molecular Properties

The new compounds, 1,3,5-tris(halogenophenylphenylamino)benzenes (*o*-, *m*-, and *p*-XTDABs (X=F, Cl, Br)) were successfully synthesized by the Ullmann reaction of 1,3,5-tris(phenylamino)benzene with corresponding halogenoiodobenzene (Scheme 2.1).

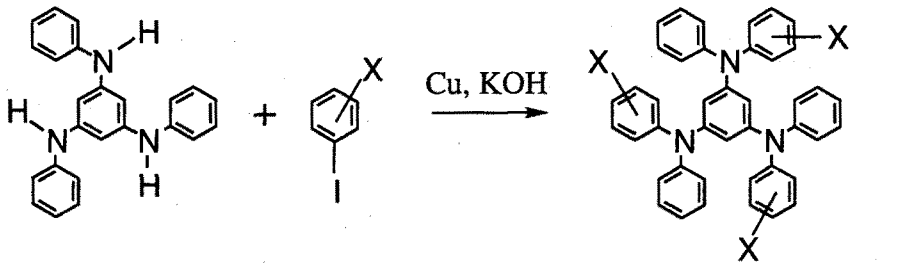


X=F ; *o*-, *m*-, *p*-FTDAB
X=Cl ; *o*-, *m*-, *p*-ClTDAB
X=Br ; *o*-, *m*-, *p*-BrTDAB

**Scheme 2.1** Synthesis of *o*-, *m*-, and *p*-XTDABs.

*o*-, *m*-, and *p*-XTDABs (X=F, Cl, Br) showed irreversible anodic oxidation processes. Table 2-1 summarizes the oxidation potentials and UV absorption maxima of

*o*-, *m*-, and *p*-XTDABs (X=F, Cl, Br).

**Table 2-1** Oxidation potentials and UV absorption maxima of *o*-, *m*-, and *p*-XTDABs (X=F, Cl, Br).

| Compound | $E^{ox}_{p/2}$ / V vs $Ag/Ag^+$ | $\lambda_{max}$ (log ε) / nm |
|---|---|---|
| *o*-FTDAB | 0.68 | 294 (4.9) |
| *m*-FTDAB | 0.74 | 299 (4.9) |
| *p*-FTDAB | 0.62 | 297 (4.9) |
| *o*-ClTDAB | 0.68 | 297 (4.9) |
| *m*-ClTDAB | 0.73 | 301 (4.9) |
| *p*-ClTDAB | 0.71 | 303 (4.9) |
| *o*-BrTDAB | 0.67 | 297 (4.8) |
| *m*-BrTDAB | 0.75 | 302 (4.9) |
| *p*-BrTDAB | 0.68 | 305 (5.0) |

## 2-4 Glass-forming Properties

*o*-, *m*-, and *p*-XTDABs (X=F, Cl, Br) were found to form readily amorphous glasses when the melt samples were cooled, whereas the parent compound 1,3,5-tris-(diphenylamino)benzene (TDAB) instantly crystallized. Figure 2-1 shows DSC curves of *p*-ClTDAB as an example. When the recrystallized sample obtained by recrystallization from toluene / hexane was heated, an endothermic peak due to melt is observed at 181 ℃. When the resulting isotropic liquid was cooled on standing in air, it formed an amorphous glassy state *via* a supercooled liquid state. When the amorphous glass sample was again heated, glass transition took place at around 64 ℃, followed by crystallization at around 112 ℃ to give the same crystal as obtained by recrystallization from toluene / hexane, which melted at 181 ℃.

The formation of the amorphous glassy state and crystalline state of XTDABs is evidenced by X-ray diffraction. Figure 2-2 shows that the X-ray diffraction patterns of the amorphous glassy state and the crystalline state of *p*-ClTDAB as an example. The X-ray diffraction pattern of the amorphous glassy state obtained by cooling the melt

sample show no sharp peak characteristic of the crystal. By contrast, characteristic sharp peaks due to crystal appear in the X-ray diffraction pattern of recrystallized sample. The formation of the amorphous glass of *p*-ClTDAB was also evidenced by polarizing microscopy. Likewise, the formation of the amorphous glasses of the other XTDABs was also evidenced by DSC, X-ray diffraction and polarizing microscopy. Thus, *o*-, *m*-, and *p*-XTDABs (X=F, Cl, and Br) constitute a new family of molecular glasses. Table 2-2 summarizes the glass-transition, crystallization, and melting temperatures ($T_g$, $T_c$, and $T_m$), and thermodynamic parameters determined by DSC [specific heat jumps at $T_g$ ($\Delta C_p$), enthalpy and entropy changes ($\Delta H$ and $\Delta S$)], and the difference between the $T_c$ and $T_g$ ($T_c$-$T_g$) for *o*-, *m*-, and *p*-XTDABs (X=F, Cl, Br).

In contrast to TDAB, which readily crystallizes even when the melt sample is rapidly cooled with liquid nitrogen, the facile glass formation for XTDABs as well as for the methyl-substituted TDABs may be ascribed to the increase in the number of conformers due to the incorporation of the halogen substituent in TDAB. Thus, increasing the number of conformers of nonplanar molecules can be a concept for molecular design of the molecular glass.

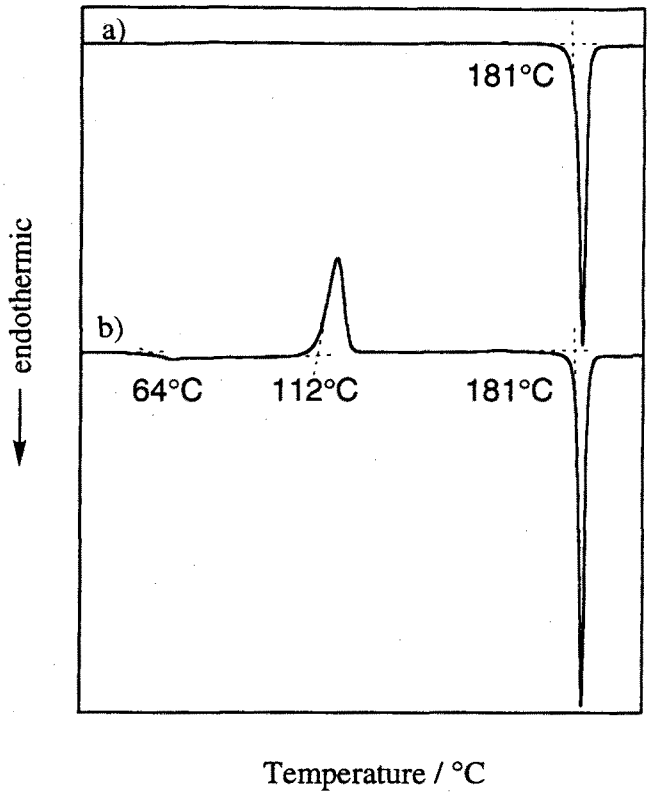


**Figure 2-1** DSC curves of *p*-ClTDAB. Heating rate; 5 °Cmin$^{-1}$. a) Crystalline sample obtained by recrystallization from toluene / hexane. b) Glass sample obtained by cooling the melt at a cooling rate of 50 °Cmin$^{-1}$.

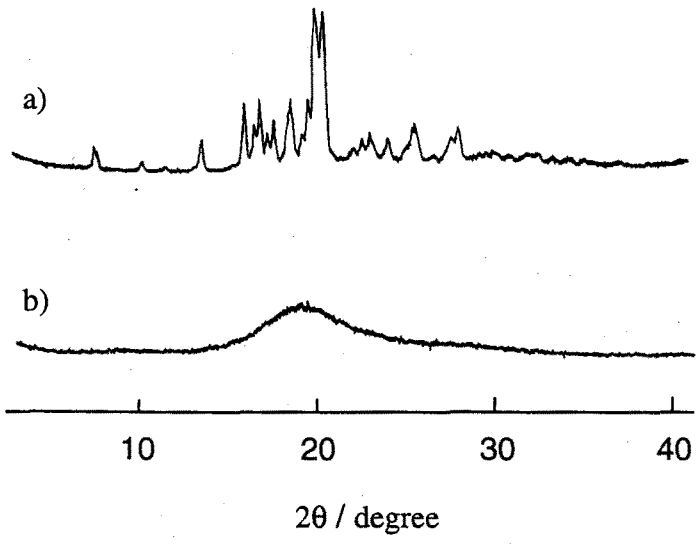


**Figure 2-2** X-Ray diffraction patterns of *p*-ClTDAB. a) Crystalline sample obtained by recrystallization from toluene / hexane. b) Glass sample obtained by cooling the melt at a cooling rate of 50 °Cmin$^{-1}$.

**Table 2-2** Glass-transition, crystallization, and melting temperatures ($T_g$, $T_c$, and $T_m$), thermodynamic parameters [specific heat jumps at $T_g$ ($\Delta C_p$), enthalpy and entropy changes ($\Delta H$ and $\Delta S$)], and the difference between $T_c$ and $T_g$ ($T_c$-$T_g$) for *o*-, *m*-, and *p*-XTDABs (X=F, Cl, Br)[a]

| Compound | $T_g$ ( $\Delta C_p$ ) | $T_c$ ( $\Delta H_c$ ) | $T_m$ ( $\Delta H_m$, $\Delta S_m$ ) | $T_c$–$T_g$ |
|---|---|---|---|---|
| | °C ( $JK^{-1}mol^{-1}$) | °C ( $kJmol^{-1}$) | °C ($kJmol^{-1}$, $JK^{-1}mol^{-1}$) | ℃ |
| *o*-FTDAB | 49 (250) | 77 (-19) | 223 (50,101) | 28 |
| *o*-ClTDAB | 49 (180) | 95 (-21) | 193 (37,79) | 46 |
| *o*-BrTDAB | 55 (140) | 123 (-30) | 186 (35,76) | 68 |
| *m*-FTDAB | 48 (250) | 80 (-23) | 215 (43,88) | 32 |
| *m*-ClTDAB | 49 (220) | 105 (—[b]) | 147 (—[b]) | 56 |
| *m*-BrTDAB | 54 (250) | —[c] | 165 (52, 119)[d] | —[c] |
| *p*-FTDAB | 54 (170) | 65 (-16) | 228 (51,102) | 11 |
| *p*-ClTDAB | 64 (220) | 112 (-26) | 181 (38,84) | 48 |
| *p*-BrTDAB | 72 (220) | —[c] | 165 (41, 94)[d] | —[c] |

[a] Glass samples were heated at a heating rate of 5°Cmin$^{-1}$.

[b] These parameters cannot be determined because the exothermic peak due to crystallization overlapped with the endothermic peak due to melting.

[c] No crystallization.

[d] Values for the crystalline samples obtained by recrystallization from toluene / hexane.

## 2-5 Striking Effect of the Kind of Halogen Substituents on the Ease of Glass formation, Glass-transition Temperature, and Stability of the Glassy State

In addition of glass formation of *o*-, *m*-, and *p*-XTDABs (X=F, Cl, Br), it was found that the halogen substituent strikingly affects the ease of glass formation, glass-transition temperature and stability of the glassy state of *o*-, *m*-, and *p*-XTDABs (X=F, Cl, Br) as follows;

(1) While FTDABs require rapid cooling of the melt samples with liquid nitrogen to form glasses, ClTDABs and BrTDABs readily produce amorphous glasses even on slow cooling of the melt samples at a cooling rate as slow as 10 ℃min$^{-1}$.

(2) The glass-transition temperature increases in the order FTDAB < ClTDAB < BrTDAB.

(3) The glassy state of FTDABs and ClTDABs is less stable than that of BrTDABs; while the glasses of *o*-, *m*-, *p*-FTDABs and *o*-, *m*-, *p*-ClTDABs tend to crystallize when allowed to stand at room temperature for a few days and for a few weeks, respectively, the glasses of *m*- and *p*-BrTDABs do not crystallize for one and a half year.

(4) The value of difference between the $T_c$ and $T_g$ increases in the order FTDAB < ClTDAB < BrTDAB. Furthermore, The *m*- and *p*-BrTDAB glasses in particular exhibit no crystallization behavior even on heating above the $T_g$s, whereas the glasses of the other compounds crystallize on heating above the $T_g$s.

Thus, the ease of glass formation, glass-transition temperature, and stability of the resulting glass were found to increase in the order FTDABs < ClTDABs < BrTDABs.

The marked effects of the halogen substituent on the ease of glass formation and stability of the glassy state observed for *o*-, *m*-, and *p*-XTDABs (X=F, Cl, Br), *i.e.*, easier glass formation and increasing stability of the resulting glass in the order F < Cl <

Br, can be explained in terms of the bulkiness and weight of the halogen atom. That is, the more bulky and heavier halogen atom will prevent easy packing of molecules and easy diffusion of molecules in the process of crystal growth, and hence prevent crystallization. These result present an important concept of molecular design for creation of molecular glasses.

## 2-6 The Relationship between Melting and Glass-transition Temperatures and Halogen Substituents

The relationship between the melting temperature ($T_m$) and $T_g$ of *o*-, *m*-, and *p*-XTDABs should be noted. Figure 2-3, Figure 2-4, and Figure 2-5 show the relationship between the $T_m$ and $T_g$, and the kind of halogen atom for *o*-, *m*-, and *p*-XTDABs (X=F, Cl, Br). Whereas the $T_m$ of XTDABs decreases in the order F > Cl > Br, the $T_g$ increases in the order F < Cl < Br.

It is generally recognized for a wide variety of amorphous materials that a empirical relationship between $T_g$ and $T_m$ exists, and the relationship is commonly expressed as $T_g \sim (2/3)T_m$ or $T_g \sim (1/2)T_m$.[41,42] That is, polymers with a high melting temperature have a high glass-transition temperature. However, the opposed trend in $T_m$ and $T_g$ was observed for XTDABs. These results indicate that the dominant factors determining the $T_g$ and $T_m$ of molecular glasses are different from those of the polymers.

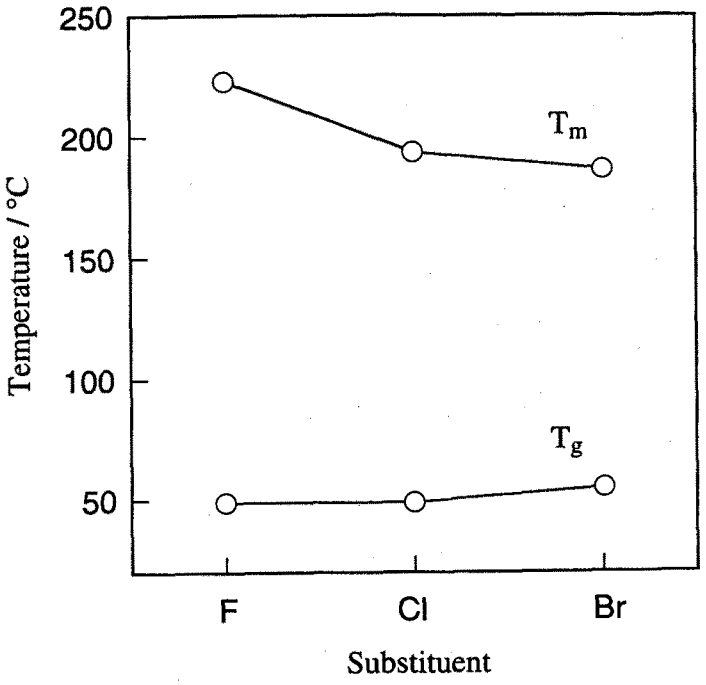


**Figure 2-3** Relationship between the melting and glass-transition temperatures, and the kind of halogen substituent for *o*-XTDABs (X=F, Cl, Br).

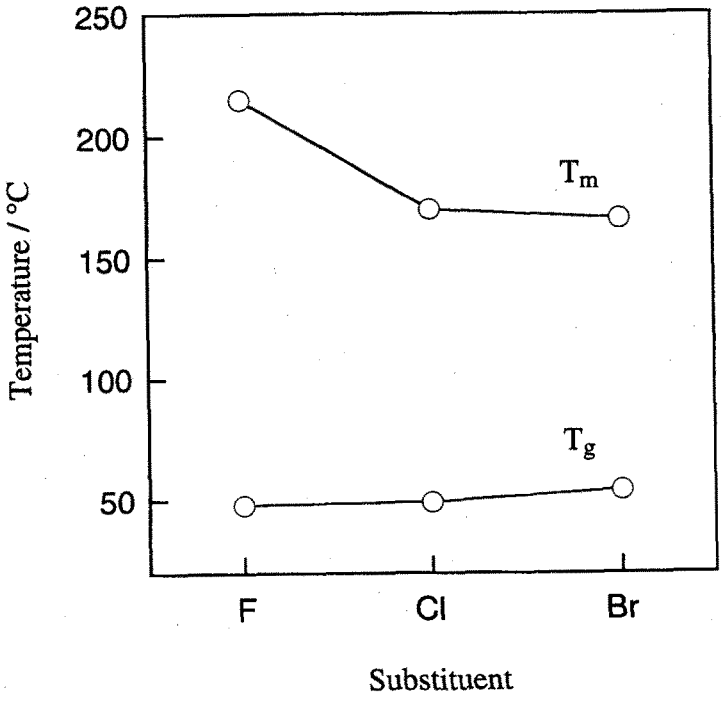


**Figure 2-4** Relationship between the melting and glass-transition temperatures, and the kind of halogen substituent for *m*-XTDABs (X=F, Cl, Br).

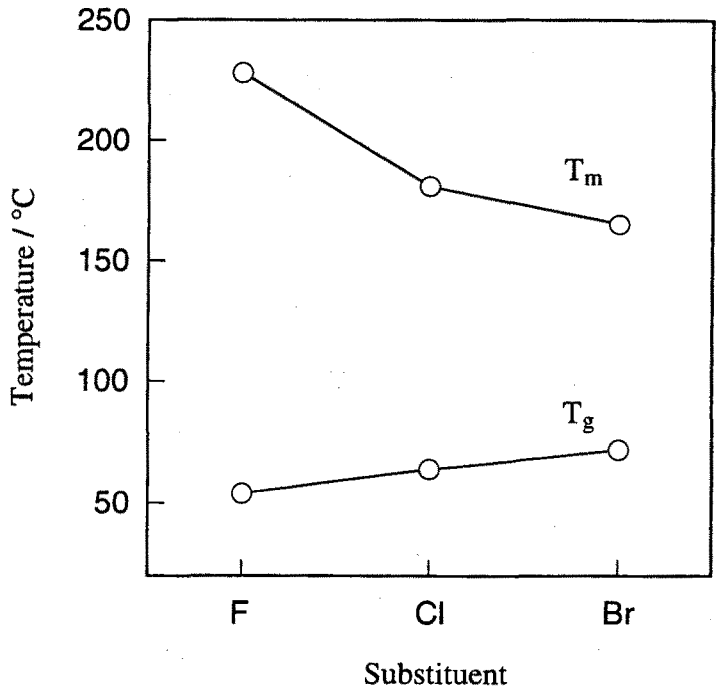


**Figure 2-5** Relationship between the melting and glass-transition temperatures, and the kind of halogen substituent for *p*-XTDABs (X=F, Cl, Br).

## 2-7 Conclusion

A new class of π-electron starburst molecules, *o*-, *m*-, and *p*-XTDABs (X=F, Cl, Br) have been designed and synthesized for making a new family of molecular glasses, and their glass-forming properties have been investigated. *o*-, *m*-, and *p*-XTDABs (X=F, Cl, Br), as well as methyl-substituted TDABs, were found to readily form amorphous glasses when cooled from the melts, whereas parent compound, TDAB dose not form an amorphous glass even when rapid cooled from the melt with liquid nitrogen. A concept of molecular design for the molecular glass is established, *i.e.*, increasing the number of conformers by incorporating substituent to nonplanar molecules lowers the symmetry of the molecule and hence prevents crystallization. It was found that the ease of glass-formation, stability of glassy state and glass-transition temperature of *o*-, *m*-, and *p*-XTDABs were greatly affected by the kind of halogen atom, increasing in the order FTDABs < ClTDABs < BrTDABs. The difference in the bulkiness and weight of halogen atom incorporated to TDAB is responsible for these results. The present study

presents an important guideline for future development of molecular glasses.

# CHAPTER 3

## Charge Transport in the Molecular Glass

### 3-1 Introduction

Charge transport in the organic disordered systems, *e.g.*, polymers and in particular molecularly-doped polymer systems where low molecular-weight organic materials are dispersed into binder polymers, has been a subject of recent application as photoreceptor materials in electrophotography.[43-59]

The mean velocity (v) of charge carriers in a material is proportional to the electric field (E), and the coefficient is defined as drift mobility ($\mu$), as described by eqn. 3-1;

$$v=\mu E \qquad (3\text{-}1)$$

The charge-carrier drift mobility ($\mu$) is generally evaluated by the time-of-flight method. The flight time ($\tau_t$), which is needed for the photogenerated carriers by irradiation of pulsed light to transport across the sample with a thickness of L under the external applied voltage (V), can be determined from the transient photocurrent. The charge-carrier drift mobility can be calculated from eqn. 3-2;

$$\mu=L^2/\tau_t V \qquad (3\text{-}2)$$

The values of the drift mobility are too small to be described by band transport , and hence it has generally been accepted that charge transport in organic disordered systems takes place by a hopping process through the intermolecular $\pi$–electron overlap. That is, the charge transport in the amorphous solid is the one-electron redox process between the neutral molecule (N) and its radical cation ($N^{\cdot +}$) or radical anion ($N^{\cdot -}$).

$$N^{\cdot +} + N \longrightarrow N + N^{\cdot +}$$
$$N^{\cdot -} + N \longrightarrow N + N^{\cdot -}$$

It is known that charge transport in organic disordered systems such as amorphous polymers and molecularly doped polymer systems generally shows the following

characteristic features: (a) the drift mobility of charge carriers is very small, being on the order from *ca.* $10^{-8}$ to $10^{-4}$ $cm^2V^{-1}s^{-1}$, (b) the transient photocurrent is dispersive as contrast to the rectangular waveform observed for single crystal, (c) the drift mobility is electric-field dependent and generally proportional to the $\exp(SE^{1/2})$, and (d) charge transport is a thermally activated process.

Scher-Montroll theory[60]

Scher and Montroll proposed the theory considers the distribution of hopping time arising from the existence of dispersion in the intersite distances and the potential barriers between the sites. Assuming the hopping-time distribution function ($\psi(t)$) of hopping time is described by eqn. 3-3, the dispersive transient photocurrent is described by eqn. 3-4;

$$\psi(t) \propto t^{-(1+\alpha)} \qquad (3\text{-}3)$$

$$\left.\begin{aligned} i_{ph} &\propto t^{-(1+\alpha)} \quad (t < \tau_t) \\ i_{ph} &\propto t^{-(1-\alpha)} \quad (t > \tau_t) \end{aligned}\right\} \qquad (3\text{-}4)$$

$$(0 < \alpha < 1)$$

The mobility in the wide range of polymers and molecularly doped polymer systems had been measured and the experimental results had been analyzed by the Scher-Montroll theory.[61]

The charge-carrier drift mobility, $\mu$ is generally dependent upon the intersite distance ($\rho$), temperature (T), and electric field (E), and described by eqn. 3-5;

$$\mu=\mu_0\rho^2\exp[f_1(\rho)]\exp[f_2(T,\rho)]\exp[f_3(E,T,\rho)] \qquad (3\text{-}5)$$

$f_1(\rho)$ represents the intermolecular wavefunction overlap, and the dependence of the charge-carrier drift mobility on the intersite distance is expressed by eqn. 3-6;

$$\mu \propto \rho^2\exp(-2\rho/\rho_0) \qquad (3\text{-}6)$$

where, $\rho_0$ is wavefunction decay constant.

A few models have been proposed to explain temperature and electric-field dependencies of drift mobilities in organic disordered systems, which include Poole-Frenkel model,[62] small-polaron model,[48–51,63] and disorder formalism.[64–71]

Poole-Frenkel Model[62]

Poole-Frenkel effect represents the exponential increase of emission current in an insulator with increasing electric field arising from the decrease of the potential barrier of trap site (Figure 3-1).

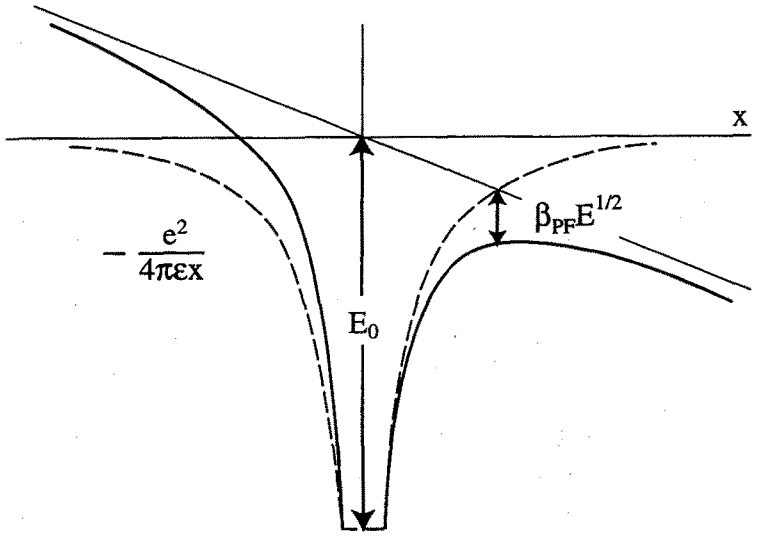


**Figure 3-1** Schematic diagram of Poole-Frenkel effect.

Gill proposed an empirical equation explains the electric-field and temperature dependencies of the charge-carrier drift mobility in the charge-transfer complex of poly(vinylcarbazole) (PVCz) / 2,4,5-trinitrofluorenone (TNF) (eqn. 3-7);

$$\mu = \mu_0 \exp\left(-\frac{E_0 - \beta_{PF}E^{1/2}}{k_B T_{eff}}\right) \qquad (3\text{-}7)$$

$$T_{eff}^{-1} = T^{-1} - T_o^{-1}$$

where $E_0$ is the activation energy at the zero electric field, $\beta_{PF}$ the Poole-Frenkel coefficient, $k_B$ the Boltzmann's constant, E the electric field, and $T_0$ the temperature at which the extrapolated data of Arrhenius plots at various electric fields intersect with one another, and $\mu_0$ the mobility at $T_0$. The electric-field and temperature dependencies of charge-carrier drift mobility in the wide range of amorphous solids are reported to be fitted to this empirical equation. However, the physical meanings of $T_0$ and $\mu_0$ have not been clarified. Furthermore, it is difficult to be accepted that the unreasonable number of Coulomb centers exist in the system.

Small-Polaron Theory[48-51,63]

In terms of the small-polaron theory, the polaron hopping rate in the absence of electric field, R is described by eqn. 3-8;

$$R = P\left(\frac{\omega_0}{2\pi}\right)\exp\left(-\frac{\varepsilon_a}{k_B T}\right) \qquad (3\text{-}8)$$

where, $\varepsilon_a$ is the energy required for deformation in order to coincide the energy between the neighboring sites, P represents the probability that a charge carrier will hop once an energy coincidence occurs, $\omega_0/2\pi$ is the frequency of energy coincidence. Eqn. 3-9 is derived from the Einstein's equation, $\mu=(e/kT)D$ (D is a diffusion coefficient) and $D=R\rho^2$;

$$\mu = \left(\frac{e}{k_B T}\right)\rho^2 P\left(\frac{\omega_0}{2\pi}\right)\exp\left(-\frac{\varepsilon_a}{k_B T}\right) \qquad (3\text{-}9)$$

The charge-carrier drift mobility is expressed by eqn. 3-10;

$$\mu = \left(\frac{e\rho^2}{k_B T}\right)P\left(\frac{\omega_0}{2\pi}\right)\exp\left(-\frac{\frac{1}{2}E_p - J}{k_B T}\right) \qquad (3\text{-}10)$$

or in terms of the parameters in eqn. 3-5,

$$\mu_0 = \frac{e\omega_0}{2\pi k_b T}$$

$$\exp[f_1(r)]=P$$

$$\exp[f_2(T,\rho)] = \exp\left(-\frac{\frac{1}{2}E_p - J}{k_B T}\right)$$

where, $E_p$ is the polaron binding energy, J the overlap integral. The temperature dependence of drift mobility is Arrhenius fashion and the activation energy is expressed as ($E_p$/2-J).

Disorder formalism[64-71]

In terms of the disorder formalism, which assumes that charge transport occurs by hopping through a manifold of localized states with superimposed energetic and positional disorders, electric-field and temperature dependencies of charge-carrier drift mobility are described by eqn. 3-11;

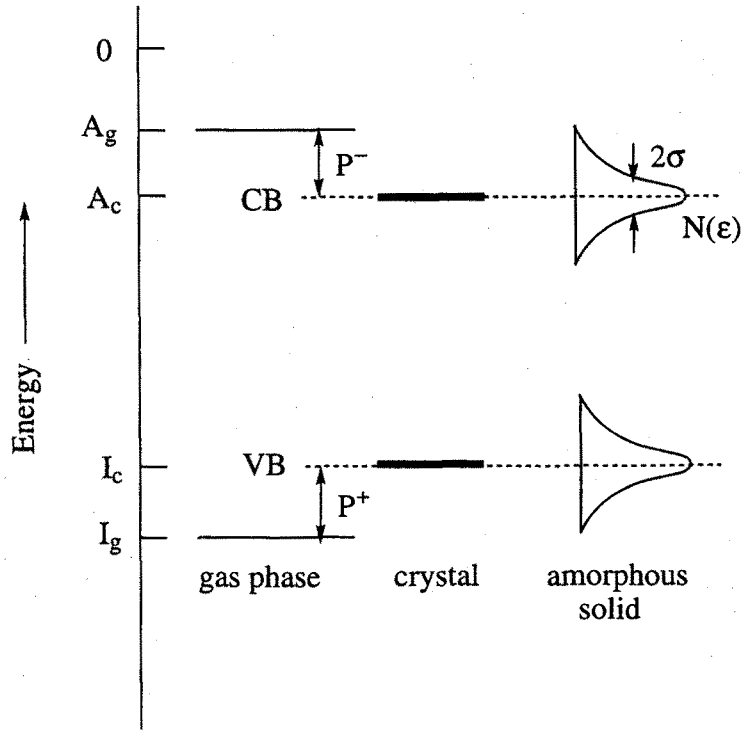


**Figure 3-2** Energy level spectrum of ionic states in molecular solids. $I_g$ and $A_g$ are the gas phase values of the ionization potential and the electron affinity, respectively. $P^+$ and $P^-$ are the polarization energies of a molecular cation and anion, respectively. σ denotes the energetic width of the distribution of states in the amorphous solid.

$$\mu(\hat{\sigma},\Sigma,E)=\begin{cases}\mu_0\exp\left[-\left(\frac{2}{3}\hat{\sigma}\right)^2\right]\exp\left[C\left(\hat{\sigma}^2-\Sigma^2\right)E^{1/2}\right] & (\Sigma\geq 1.5)\\ \mu_0\exp\left[-\left(\frac{2}{3}\hat{\sigma}\right)^2\right]\exp\left[C\left(\hat{\sigma}^2-2.25\right)E^{1/2}\right] & (\Sigma<1.5)\end{cases} \qquad (3\text{-}11)$$

$$\hat{\sigma}=\frac{\sigma}{k_BT},\quad \sigma=\frac{3}{2}k_BT_0$$

where $\sigma$ represents the energetic disorder, *i.e.*, diagonal disorder, is the width of the Gaussian density of states, $\Sigma$ a parameter that characterizes the degree of the positional disorder, *i.e.*, off-diagonal disorder, $\mu_0$ a hypothetical mobility in the disorder-free system, E the electric field, and C an empirical constant.

The charge-carrier drift mobility depends on the intersite distance ($\rho$), and the dependence of the activation energy on $\rho$ can be explained in terms of the small polaron theory. The dependencies of charge-carrier drift mobility and the activation energy on $\rho$ for 4-diethylaminobenzaldehyde diphenylhydrazone (DEH) and N,N'-diphenyl-N,N'-bis(3-methylphenyl)-[1,1'-biphenyl]-4,4'-diamine (TPD) doped in polycarbonate (PC) were reported. For the DEH / PC system, the activation energy $\varepsilon_p$ is independent on $\rho$ and the P is dependent on $\rho$, consistent with nonadiabatic small polaron hopping. On the other hand, for the TPD / PC system, the activation energy is dependent on $\rho$ and the P is independent on $\rho$, consistent with adiabatic small polaron hopping.[48] The transition from adiabatic to nonadiabatic small polaron hopping had been also observed. For the tri(*p*-tolyl)amine doped in PC system, adiabatic small polaron hopping was observed for the concentration of 50 wt% ~ 10 wt%, and nonadiabatic small polaron hopping was observed for the concentration less than 10 wt%.[50]

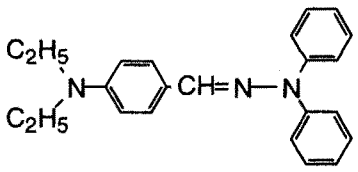

DEH

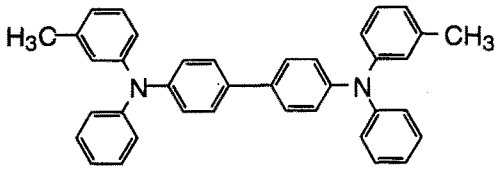

TPD

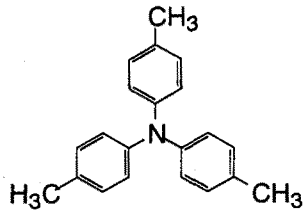

tri(*p*-tolyl)amine

There has been few examples of electron transporting materials so far. Very recently, some studies of electron transport have been reported. For instance, electron mobilities have been reported in the following systems; 4-*n*-butoxycarbonyl-9-fluorenylidene malononitrile (doped in polyester at 30 wt%; $\mu_e$ = $1.0x10^{-7}$ $cm^2V^{-1}s^{-1}$ at an electric field of $4x10^5$ $Vcm^{-1}$ at 300 K),[54,72] N,N'-bis(2-phenethyl)-perylene-3,4:9,10-bis(dicarboximide) (PECI; vapor deposited film; $\mu_e$ = $5.0x10^{-4}$ $cm^2V^{-1}s^{-1}$ at $2.0x10^5$ $Vcm^{-1}$ at 300 K),[73] and 3,5-dimethyl-3',5'-di-*tert*-butyl-4,4'-diphenoquinone (DPQ; doped in PC at 35 wt%; $\mu_e$=$2.0x10^{-7}$ $cm^2V^{-1}s^{-1}$ at an electric field of $2.0x10^5$ $Vcm^{-1}$ at 293 K).[74,75]

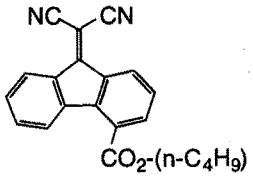

4-*n*-butoxycarbonyl-9-fluorenylidene malononitrile

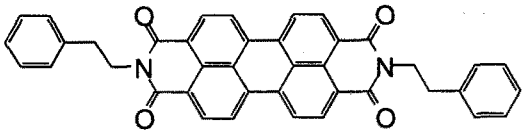

PECI

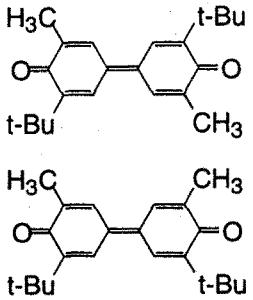

DPQ

It has recently been revealed that charge transport in molecularly doped polymer systems, where the binder polymer was thought to be inert for charge transport, is greatly affected by the binder polymer.[76-78] In fact, hole drift mobilities in the molecularly doped polymer systems have been reported to vary by two orders of magnitude depending upon the binder polymer; for instance, hole drift mobility of TPD doped in polystyrene at 10 wt% is *ca.* $10^{-8}$ $cm^2V^{-1}s^{-1}$ in contrast to the mobility doped in polycarbonate at 10 wt% is *ca.* $10^{-10}$ $cm^2V^{-1}s^{-1}$. Charge-dipole interactions between a charge on the transport molecule and the binder polymer are thought to cause fluctuation of hopping site energies and change in the molecular overlap integral. This binder effects is evidenced by the study of charge transport of TAPC doped in poly(styrene)s substituted H, *tert*-buthyl, and chlorine. The hole drift mobility decreased in the order of $6x10^{-4}$ $cm^2V^{-1}s^{-1}$ (H), $4x10^{-4}$ $cm^2V^{-1}s^{-1}$ (*p-tert*-butyl), and $6x10^{-5}$ $cm^2V^{-1}s^{-1}$ (*p*-Cl). The diagonal disorder, $\sigma$ value increased in the same order, in spite of the fact that the $\Sigma$ and $\mu_0$ are almost the same among these systems. That is, the difference in $\sigma$ is responsible for the difference in the $\mu_h$, and $\sigma$ value increases with increasing dipole moment of the polymer. The increase in the fluctuation of electrostatic potential with increasing dipole moment of the polymer is thought to be responsible for the increase in $\sigma$ value.[79-81]

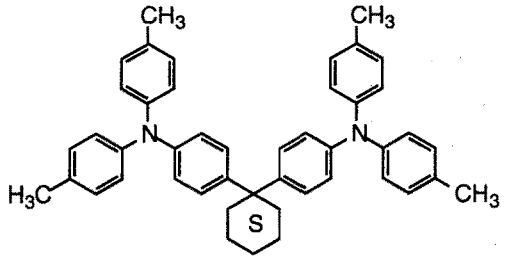


TAPC

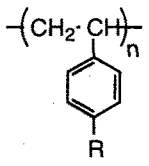


R=H, t-Bu, Cl

The charge transport in molecularly doped polymer system in the presence of a polar additive has been reported in order to elucidate the effect of polarity on charge transport properties.[82] The hole drift mobility of TAPC (75 wt%) doped in polycarbonate (PC; 23 wt%) in the presence of *o*-, *m*-, and *p*-dinitrobenzene (*o*-, *m*-,

*p*-DNB; 2 wt%) as a polar additive decreased monotonically in the series TAPC / PC, TAPC (*p*-DNB) / PC, TAPC (*m*-DNB) / PC, and TAPC (*o*-DNB) / PC, following the dipole moments of the additive which were 0.5 D (*p*-DNB), 4 D (*m*-DNB), and 6 D (*o*-DNB), respectively. However, the $\sigma$ values of the three components systems were almost the same; this means the polar group that is located next to the charged center will contribute significantly to the fluctuation of the electrostatic potential.

In order to clarify intrinsic charge-transport properties of low molecular weight organic materials in the disordered system, it is desirable to investigate charge transport in the amorphous glassy state of low molecular-weight organic materials without a binder polymer. However, very few studies have been made of charge transport in the amorphous glassy state of low molecular-weight organic materials, because there were very few known examples of low molecular-weight organic compounds that form stable glasses with relatively high glass-transition temperatures. Very recently, papers dealing with charge transport in amorphous films of low molecular-weight materials have began to appear.[22,25-30,38,39,84]

We have been studying the synthesis, properties, and applications of low molecular-weight organic compounds that readily form stable amorphous glasses above room temperature. We have designed and synthesized several novel families of molecular glasses based on $\pi$-electron systems and studied charge transport in the molecular glasses, *e.g.*, 1,3,5-tris[4-(3-methylphenylphenylamino)phenyl]benzene (*m*-MTDAPB),[22] tri(biphenyl-4-yl)amine (TBA),[25,26] 4-diphenylaminobenzaldehyde methylphenylhydrazone (DPMH), 4-diphenylaminoacetophenone diphenylhydrazone (M-DPH), and 4-diphenylaminobenzaldehyde diphenylhydrazone (DPH).[27-30]

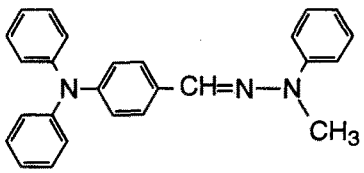


DPMH

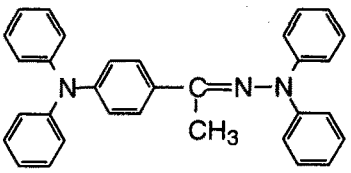


M-DPH

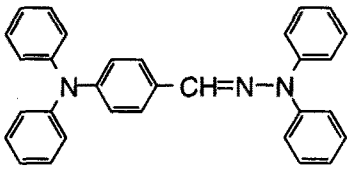


DPH

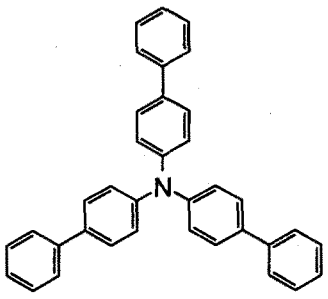


TBA

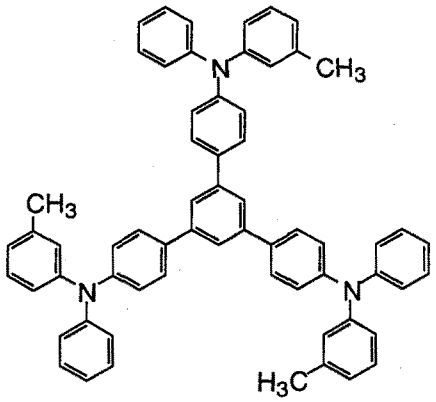


*m*-MTDAPB

For the purpose of establish the molecular design for molecular glasses with high charge-carrier drift mobility, it is important to study the relationship between molecular structure and charge transport properties. We report here charge transport in the molecular glass of tris[4-(2-thienyl)phenyl]amine (TTPA) and in the molecular glasses of tri(*o*-terphenyl-4-yl)amine (*o*-TTA), tri(*m*-terphenyl-4-yl)amine (*m*-TTA), and tri(*p*-terphenyl-4-yl)amine (*p*-TTA). The hole drift mobility in the TTPA molecular glass was found to be higher than those of molecularly-doped polymer systems and molecular glasses which we previously studied. The hole drift mobilities in the molecular glasses of *o*-, *m*-, and *p*-TTA are greatly affect by the structure of terphenyl moiety. The effect of internal rotation on the charge transport property is discussed. Finally, we describe the first observation of negative electric-field dependence of charge-carrier drift mobility for the *o*-TTA molecule glass without a polymer binder.

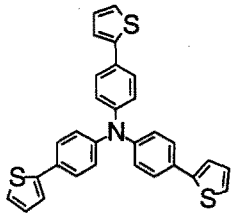

TTPA

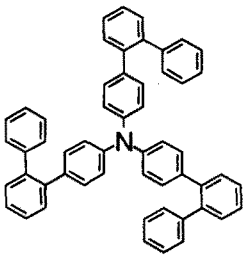

*o*-TTA

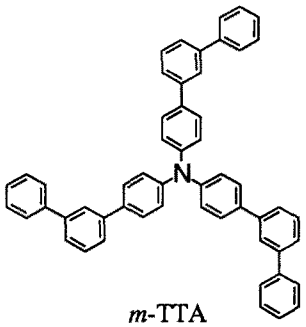

*m*-TTA

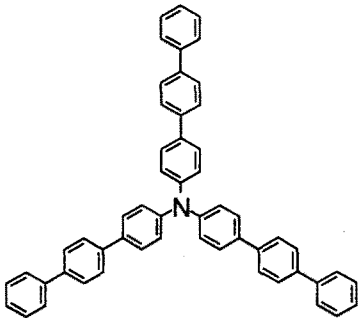

*p*-TTA

## 3-2 Charge Transport in the Molecular Glass of TTPA

Measurement

Hole drift mobility was measured by a time-of-flight method using a layered device which consists of a charge-carrier generation layer (CGL) and a charge-carrier transport layer (CTL). An appropriate amount of TTPA was melted on an ITO glass to form a film of 10 ~ 20 μm thickness, and pressed onto another ITO glass on which X-type metal free phthalocyanine dispersed in poly(ethylene-*co*-vinylchloride) as CGL was coated by a spin-coat method. A polyimide spacer was used to achieve a uniform thickness. The thickness of the sample was measured with a micrometer. The cell was mounted in a cryostat and irradiated with pulsed white light through a UV-37 glass filter (Toshiba Corp.) from a xenon stroboscopic lamp (pulse duration time : 1 ~ 4 μs). The temperature of the sample was controlled by a temperature controller, ITC 502 (Oxford). Hole carriers photogenerated in the CGL are injected into the CTL at time zero and transported across the TTPA layer under an external electric field. The photocurrent was converted to the voltage using an amplifier, LI-76 (NF Circuit), and monitored using a digital storage scope, KDS-102 (Kawasaki Electronica).

Apparatus

For the measurement of hole drift mobilities, voltage was applied to the layered device using a Takasago TMD0360-022 regulated DC power supply.

Results and discussion

The transient photocurrent observed for the TTPA glass was nearly nondispersive, as shown in Figure 3-3. The transit time ($\tau_t$) was determined from the plot of log $i_{ph}$ *vs.* log t, where $i_{ph}$ and t represent transient photocurrent and time, respectively, according to the Scher-Montroll theory.[60] The hole drift mobility was calculated from the transit time ($\tau_t$) from the equation $\mu = L^2/\tau_t V$, where L is the thickness of CTL and V the applied voltage.

The hole drift mobility of TTPA in the glassy state was measured in the temperature range from 108 K to 193K. The hole drift mobility of TTPA in the glassy state at an electric field of $1.0 \times 10^5$ $Vcm^{-1}$ was determined to be $3.1 \times 10^{-6}$ and $6.4 \times 10^{-4}$ $cm^2V^{-1}s^{-1}$ at 108 K and 193 K, respectively.

The electric-field and temperature dependencies of the hole drift mobility of the TTPA glass were analyzed in terms of both the eqn. 3-7 and eqn. 3-11.

Figure 3-4 shows that the electric-field dependence of the hole drift mobility in the TTPA glass follows $\exp(SE^{1/2})$.

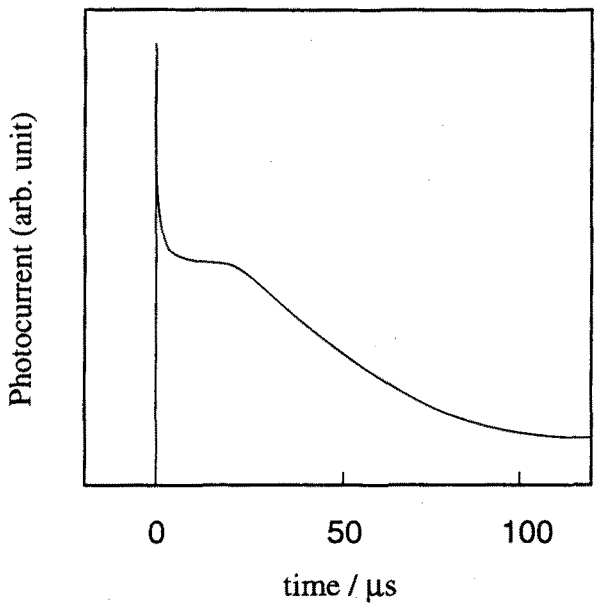


**Figure 3-3** Typical transient photocurrent observed for a TTPA glass.

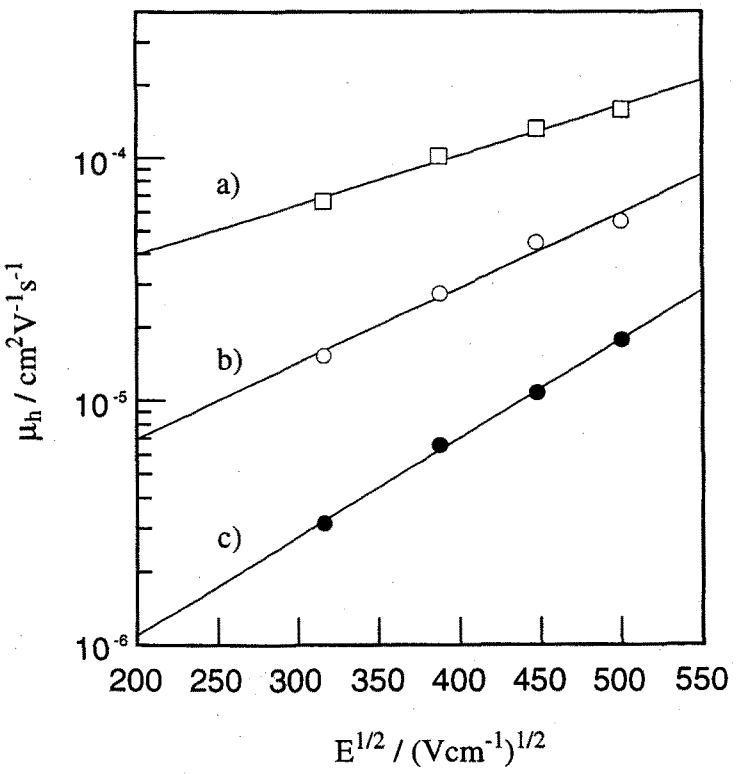


**Figure 3-4** Electric-field dependencies of the hole drift mobility of the TTPA glass at different temperatures: a) 148 K, b) 128 K, and c) 108 K.

The temperature dependence of the hole drift mobility was found to be fitted to both eqn. 3-7 and eqn. 3-11. Figure 3-5 shows Arrhenius plots of the hole drift mobility of the TTPA glass at several electric fields. The apparent activation energy ($E_{act}$) for charge transport at each electric field was obtained from the slope of the linear plots. The activation energy at the zero electric field ($E_0$) was determined by extrapolating the plot of $E_{act}$ *vs.* $E^{1/2}$ to the zero-electric field, as shown in Figure 3-6.

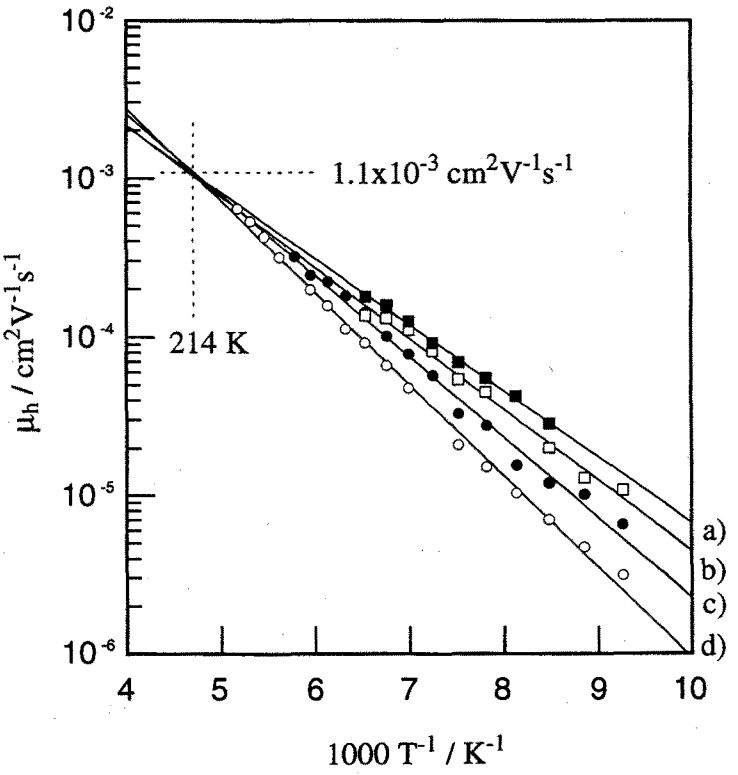


**Figure 3-5** Arrhenius plots of the hole drift mobility of the TTPA glass at different electric fields: a) 2.5 x $10^5$, b) 2.0 x $10^5$, c) 1.5 x $10^5$, d) 1.0 x $10^5$ $Vcm^{-1}$.

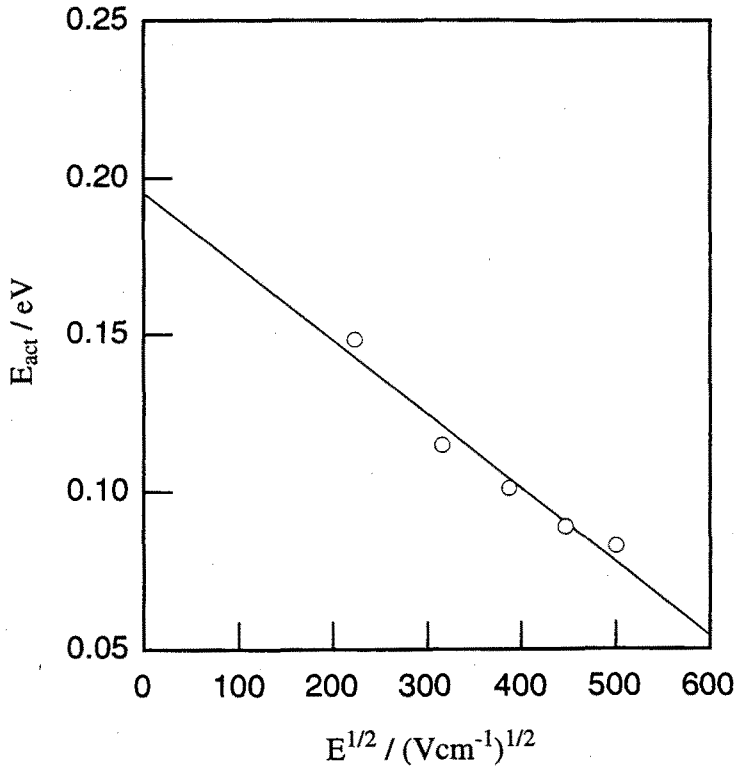


**Figure 3-6** Plots of activation energies ($E_{act}$) *vs.* $E^{1/2}$.

Figure 3-7 shows the plots of log $\mu(E=0)$ *vs.* $T^{-2}$ for the TTPA glass, where $\mu(E=0)$ is the hole drift mobility at the zero-electric field determined by extrapolating the plots of log $\mu$ *vs.* $E^{1/2}$ to the zero electric field. The parameters $\sigma$ and $\mu_0$ were obtained from the slope and the intercept, respectively, of the linear plots extrapolated to $T\rightarrow\infty$. Eqn. 3-11 predicts that the slope of the electric-field dependence of hole drift mobilities ($S=\partial\ln(\mu/\mu_0)/\partial E^{1/2}$) should be linearly dependent upon $\hat{\sigma}^2$ with a slope of C. Figure 3-8 shows the plots of S *vs.* $\hat{\sigma}^2$. As predicted, a linear relationship was observed, and the value $\Sigma$ was determined from the intersection of the linear plots at S=0, where $\hat{\sigma}^2=\Sigma^2$ holds.

The charge transport parameters in Eqn. 3-7, $\mu_0$, $E_0$, $T_0$, and $\beta_{PF}$, and those in Eqn. 3-11, $\mu_0$, $\sigma$, $\Sigma$, and C, for TTPA are summarized in Table 3-1.

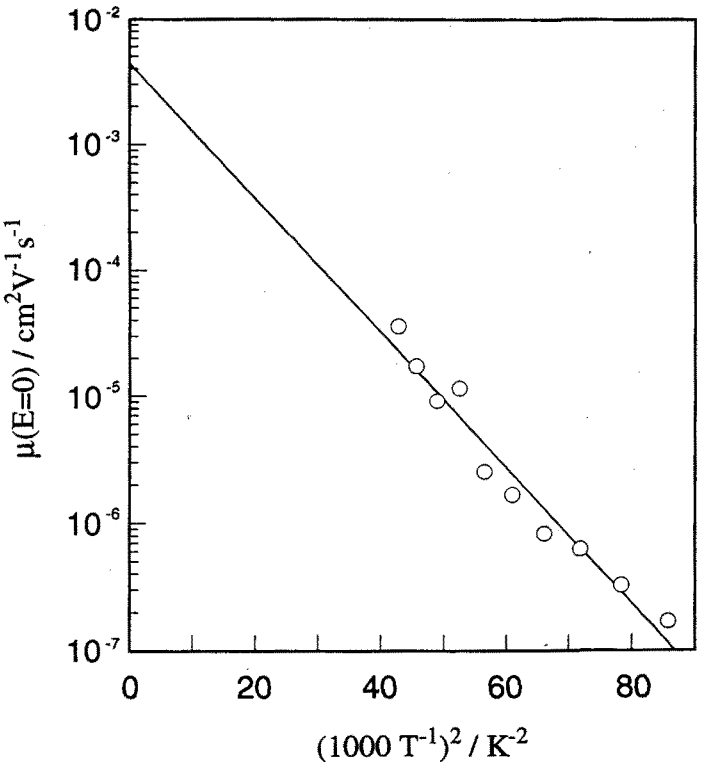


**Figure 3-7** Temperature dependence of hole drift mobilities at the zero electric field.

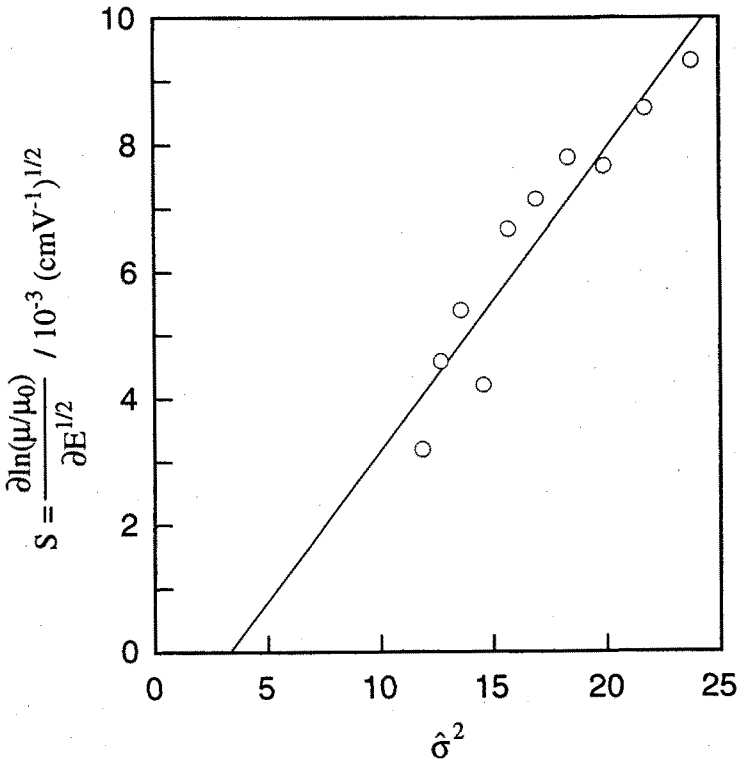


**Figure 3-8** Plots of S *vs.* $\hat{\sigma}^2$. Here, $S=\partial \ln(\mu/\mu_0)/\partial E^{1/2}$ and $\hat{\sigma}=\sigma/k_BT$.

**Table 3-1** Hole-transport parameters for the TTPA glass based on Eqn. 3-7 and Eqn. 3-11.

Based on Eqn. 3-7

$\mu_0 = 1.1 \times 10^{-3}$ cm$^2$V$^{-1}$s$^{-1}$ $E_0 = 0.19$ eV $T_0 = 214$ K $\beta_{PF} = 2.3 \times 10^{-4}$ eV(cmV$^{-1}$)$^{1/2}$

Based on Eqn. 3-11

$\mu_0 = 4.4 \times 10^{-3}$ cm$^2$V$^{-1}$s$^{-1}$ $\sigma = 0.045$ eV $\Sigma = 1.8$ $C = 4.7 \times 10^{-4}$ (cmV$^{-1}$)$^{1/2}$

It was found that the TTPA glass exhibits a hole drift mobility of $6.4 \times 10^{-4}$ cm$^2$V$^{-1}$s$^{-1}$ at an electric field of $1.0 \times 10^5$ Vcm$^{-1}$ at 193 K. This is a high value among organic disordered systems. We have shown that the glasses of tri(biphenyl-4-yl)amine and 4-diphenylaminobenzaldehyde diphenylhydrazone (DPH) exhibit hole drift mobilities of $2.9 \times 10^{-6}$ and $3.1 \times 10^{-6}$ cm$^2$V$^{-1}$s$^{-1}$, respectively, under the same conditions. The hole drift mobilities in molecularly doped polymer systems are $4.6 \times 10^{-8}$ cm$^2$V$^{-1}$s$^{-1}$ for 50 wt% DPH-doped polycarbonate system at $1.0 \times 10^5$ Vcm$^{-1}$ at 200 K and $2 \times 10^{-8}$ cm$^2$V$^{-1}$s$^{-1}$ for the 40 wt% tri(*p*-tolyl)amine-doped polycarbonate system at an electric field of $9 \times 10^4$ Vcm$^{-1}$ at 218 K.[52] The higher mobilities of molecular glasses than those of molecularly doped polymer systems are thought to be due to shorter intersite distances and less fluctuations of hopping site energies. The hole drift mobility of TTPA is found to be higher than those for other molecular glasses. It is thought that the smaller values of $E_0$ in terms of eqn. 3-7 and $\sigma$ in terms of eqn. 3-11 are partly responsible for higher charge-carrier mobility of the TTPA glass, and that the molecular structure plays an important role in the hole transport properties of molecular glasses. Further studies are in progress to investigate charge transport in a wider temperature range.

## 3-3 Charge Transport in the Molecular Glass of Tri(terphenyl-4-yl)amines

Measurement

The hole drift mobility was measured by a time-of-flight method using a layered device consisting of a charge-carrier generation layer (CGL) and a charge-carrier transport layer (CTL). An appropriate amount of material was heated melted on an indium-tin-oxide(ITO) coated glass to form a film, and pressed by another ITO glass, on which a thin film of anthra[2",1",9":4,5,6:6",5",10":4',5',6']diisoquino[2,1-a:2',1'-a']dibenz-imidazole-10,21-dione is coated by vapor deposition as a CGL, and then cooled down on standing in air. A polyimide spacer was used to achieve a uniform thickness. The thickness of the sample was measured with a micrometer. Thickness of the sample was 10-20 μm. The cell was mounted in a cryostat and irradiated with pulsed light of the wavelength longer than 600 nm from a xenon stroboscopic lamp (pulse duration time : *ca.* 1-4 μs). The temperature of the sample was controlled by a temperature controller, ITC 502 (Oxford). Hole carriers photogenerated in the CGL are injected into the CTL at time zero and transported across the CTL under an external electric field. The photocurrent was converted to the voltage using an amplifier, LI-76 (NF Circuit), and monitored using a digital storage scope, TDS540A (Tektronix).

Apparatus

For the measurement of hole drift mobilities, voltage was applied to the layered device using a Takasago TMD0360-022 regulated DC power supply. Refractive index in the glassy state was measured using Abbe refractmeter (Atago model 4T).

Figure 3-5 shows a typical transient photocurrent observed for a *m*-TTA glass at 295 K. The transient photocurrents observed for *o*-, *m*-, and *p*-TTA glasses were nearly nondispersive. The transit time ($\tau_t$) was observed as a plateau in the trace of photocurrent ($i_{ph}$) as a function of time (t), which was almost in accord with the value determined from the plot of log $i_{ph}$ *vs.* log t based on the Scher-Montroll theory.[60] The hole drift mobility was calculated from the transit time, according to the expression $\mu=L^2/\tau_t V$, where L is the sample thickness and V the applied voltage.

Table 3-2 lists the hole drift mobilities ($\mu_h$) at an electric field of $1.0\times10^5$ $Vcm^{-1}$ at 293 K together with intersite distances ($\rho$) of *o*-TTA, *m*-TTA, and *p*-TTA glasses. The hole drift mobilities in the glassy state of *o*-TTA and *p*-TTA were found to be almost the same, being more than one order of magnitude higher than that of *m*-TTA in the same conditions.

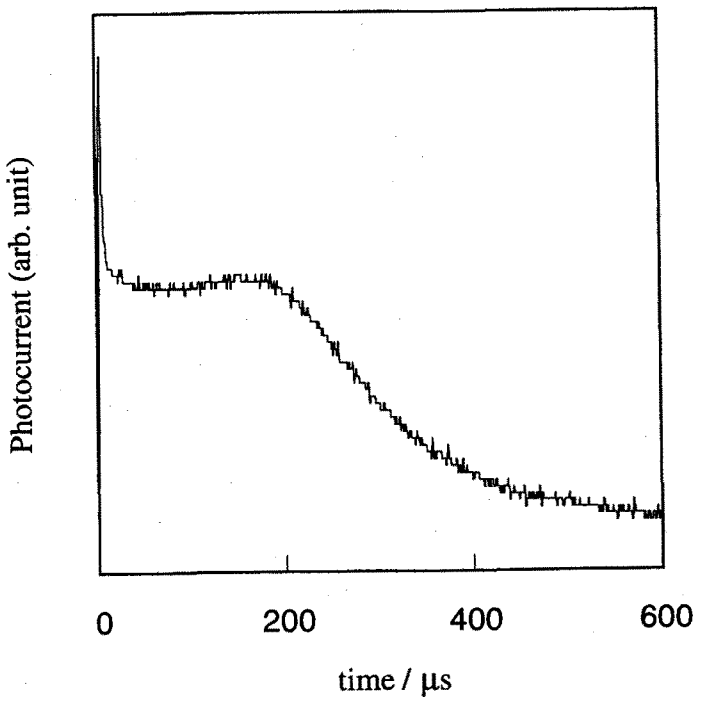


**Figure 3-9** A typical transient photocurrent observed for a *m*-TTA glass at 295 K. Thickness of the sample: 12μm; Applied voltage: 240 V.

**Table 3-2** Hole drift mobilities ($\mu_h$) and intersite distances ($\rho$) for *o*-, *m*-, and *p*-TTA

| Material | $\mu_h$ / $cm^2V^{-1}s^{-1}$ [a] | $\rho$ / Å [b] |
|---|---|---|
| *o*-TTA | $7.9x10^{-4}$ | 10.1 |
| *m*-TTA | $2.3x10^{-5}$ | 10.0 |
| *p*-TTA | $8.8x10^{-4}$ | 10.0 |

[a] Measured at an electric field of $1.0x10^5$ $Vcm^{-1}$ at 293 K.
[b] Calculated from the equation of $\rho=(M/Ad)^{1/3}$, where M is the molecular weight, A the Avogadro's number, and d the density.

Electric-field and temperature dependencies of hole drift mobilities in the *o*-, *m*-, and *p*-TTA glasses were analyzed both by the eqn. 3-7 and eqn. 3-11.

The hole drift mobilities in the *o*-, *m*-, and *p*-TTA glasses can be described by the electric-field dependence of $\exp(SE^{1/2})$. Figure 3-10 shows electric-field dependencies of the hole drift mobilities of *m*-TTA at various temperatures as an example.

First, temperature dependence of the hole drift mobilities in *o*-, *m*-, and *p*-TTA glasses was analyzed by eqn. 3-7. Figure 3-11, Figure 3-12, and Figure 3-13 show Arrhenius plots of the hole drift mobilities in *o*-, *m*-, and *p*-TTA, respectively, at varying electric fields. Those plots intersect with one another at $T_0$. No significant correlation between $T_0$ and $T_g$ has been observed. The apparent activation energy ($E_{act}$) for charge transport at each electric field is obtained from the slope of the plots for each electric field. The activation energy at the zero-electric field ($E_0$) in eqn. 3-7 was determined by extrapolation of the plots of $E_{act}$ *vs.* $E^{1/2}$ to zero-electric field, as shown in Figure 3-14. The hole transport parameters in eqn. 3-7, $\mu_0$, $E_0$, $T_0$ and $\beta_{PF}$ are summarized in Table 3-3.

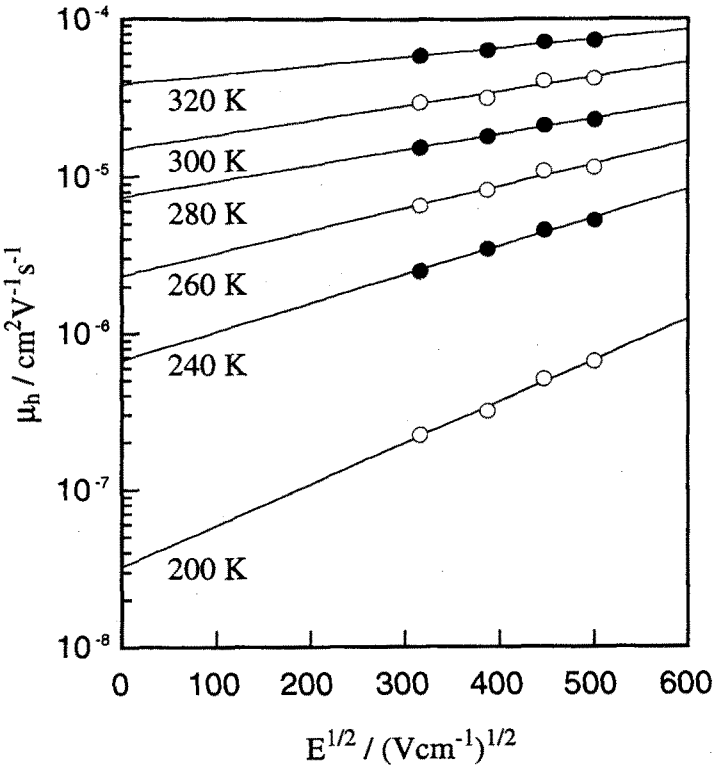


**Figure 3-10** Electric-field dependencies of hole drift mobility for a *m*-TTA glass at different temperatures.

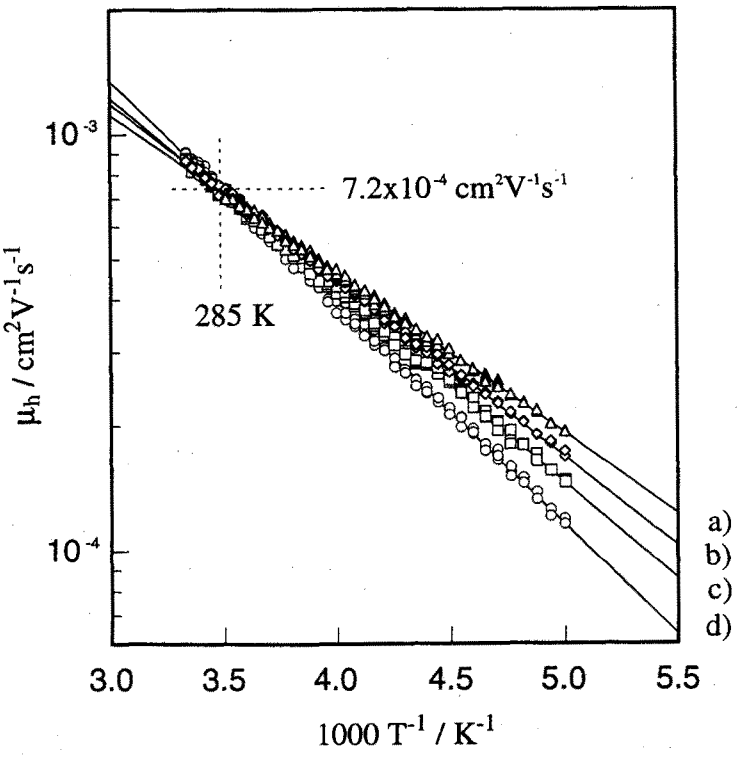


**Figure 3-11** Temperature dependencies of hole drift mobility for a *o*-TTA glass: a) $2.0x10^5$, b) $1.5x10^5$, c) $1.0x10^5$, d) $5.0x10^4$ $Vcm^{-1}$.

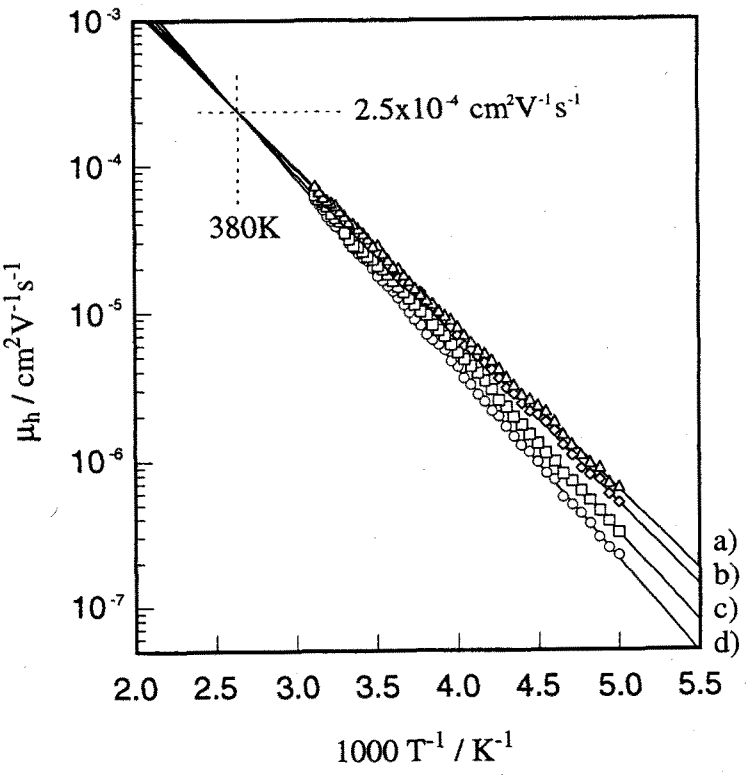


**Figure 3-12** Temperature dependencies of hole drift mobility for a *m*-TTA glass: a) $2.5x10^5$, b) $2.0x10^5$, c) $1.5x10^5$, d) $1.0x10^5$ $Vcm^{-1}$.

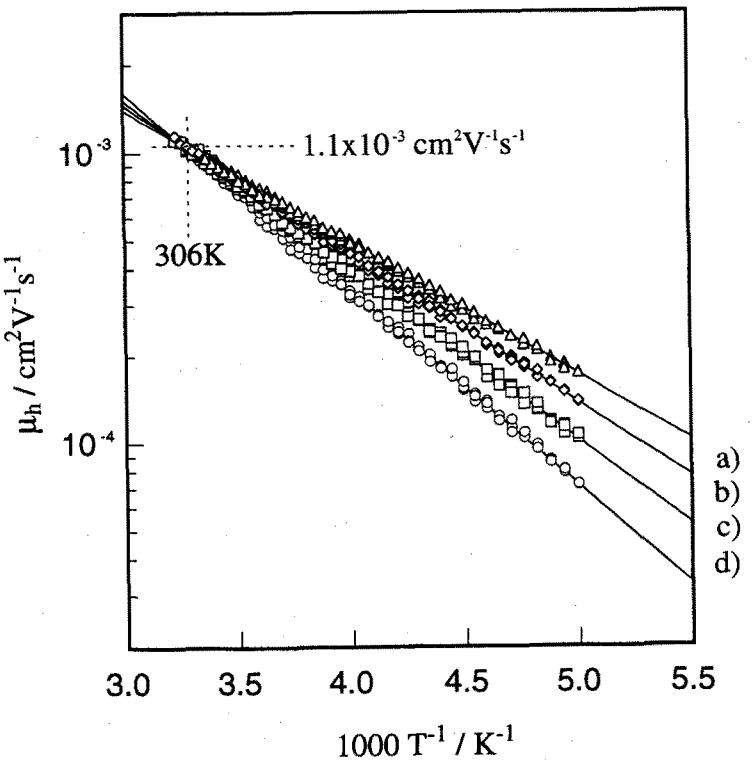


**Figure 3-13** Temperature dependencies of hole drift mobility for a *p*-TTA glass: a) $2.0x10^5$, b) $1.5x10^5$, c) $1.0x10^5$, d) $5.0x10^4$ $Vcm^{-1}$.

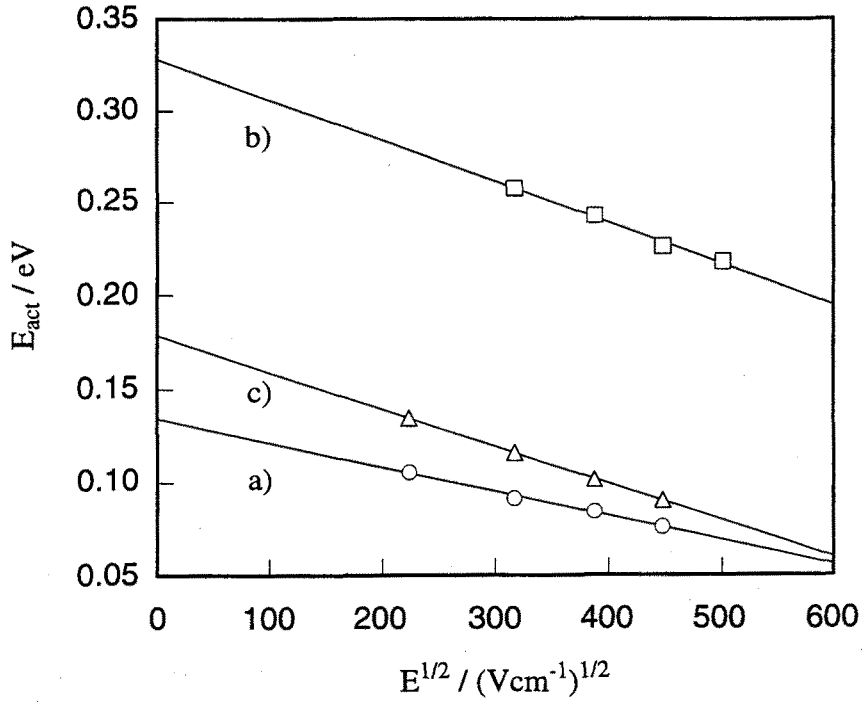


**Figure 3-14** Electric field dependencies of activation energy for a) *o*-TTA, b) *m*-TTA, and c) *p*-TTA.

**Table 3-3** Hole transport parameters based on Eqn. 3-7

| Material | $\mu_0$ / $cm^2V^{-1}s^{-1}$ | $T_0$ / K | $E_0$ / eV | $\beta_{PF}$ / $eV(cmV^{-1})^{1/2}$ |
|---|---|---|---|---|
| *o*-TTA | $7.2x10^{-4}$ | 285 | 0.13 | $1.3x10^{-4}$ |
| *m*-TTA | $2.5x10^{-4}$ | 380 | 0.33 | $2.2x10^{-4}$ |
| *p*-TTA | $1.1x10^{-3}$ | 306 | 0.18 | $2.0x10^{-4}$ |

Second, temperature dependence of hole drift mobilities was analyzed by eqn. 3-11. Figure 3-15 shows the plots of log $\mu(E=0)$, which was obtained from the plots of log $\mu$ *vs.* $E^{1/2}$ by extrapolating to zero-electric field, *vs.* $T^{-2}$ for *o*-, *m*-, and *p*-TTA glasses. The temperature dependencies of hole drift mobility at zero-electric field of *o*-, *m*-, and *p*-TTA showed a discontinuity at low temperatures. This phenomenon is thought to be

the nondispersive-to-dispersive transition, as predicted by the disorder formalism.[85] Eqn. 2 is valid only for above the nondispersive-to-dispersive transition temperature. The hole transport parameters in eqn. 3-11, $\sigma$ and $\mu_0$ were obtained from the slope and the intersection of the linear plots extrapolated to $T \rightarrow \infty$, respectively. Eqn. 3-11 predicts that slopes of the electric-field dependencies ($S=\partial \ln(\mu/\mu_0)/\partial E^{1/2}$) should be linear dependent upon $\hat{\sigma}^2$ with a slope given as C. Figure 3-16 shows the plots of $\Sigma$ *vs.* $\hat{\sigma}^2$. As predicted, a linear dependence is observed. From the S=0 intersection, $\Sigma$ can be determined from the condition $\hat{\sigma}^2=\Sigma^2$. The hole transport parameters in eqn. 3-11, $\mu_0$, $\sigma$, $\Sigma$, and C are summarized in Table 3-4.

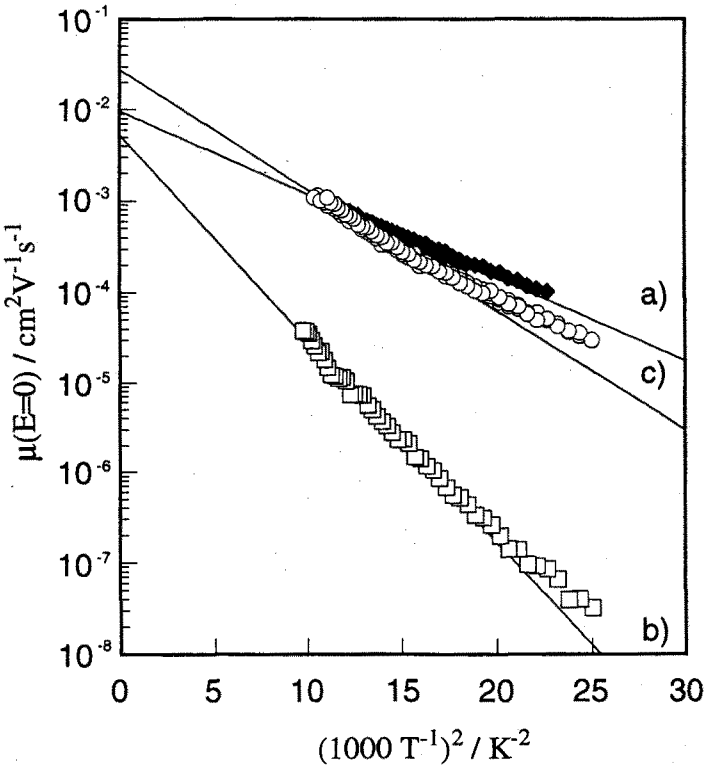


**Figure 3-15** Temperature dependencies of hole drift mobilities at zero-electric field; a) *o*-TTA, b) *m*-TTA, and c) *p*-TTA.

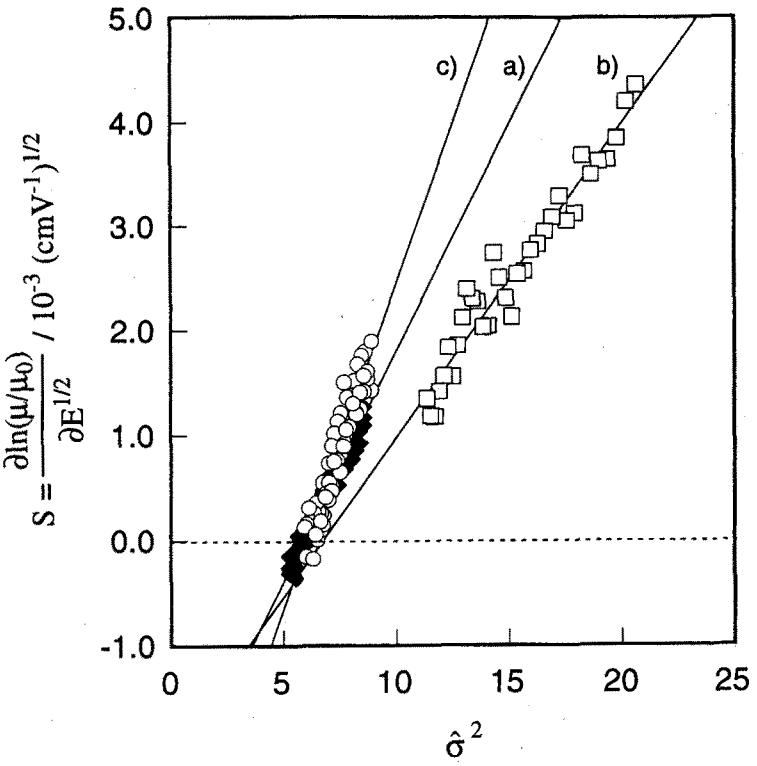


**Figure 3-16** Plots of S vs $\hat{\sigma}^2$. Here, $S=\partial \ln(\mu/\mu_0)/\partial E^{1/2}$ and $\hat{\sigma}=\sigma/k_BT$.

**Table 3-4** Hole transport parameters based on eqn. 3-11

| Material | $\mu_0$ / $cm^2V^{-1}s^{-1}$ | $\sigma$ / eV | $\Sigma$ | C / $(cmV^{-1})^{1/2}$ |
|---|---|---|---|---|
| *o*-TTA | $9.7x10^{-3}$ | 0.059 | 2.4 | $4.4x10^{-4}$ |
| *m*-TTA | $5.3x10^{-3}$ | 0.093 | 2.6 | $3.0x10^{-4}$ |
| *p*-TTA | $2.8x10^{-2}$ | 0.071 | 2.5 | $6.2x10^{-4}$ |

We have reported the charge transport property of tri(biphenyl-4-yl)amine (TBA), which is a chemical analogue of *o*-, *m*-, and *p*-TTA, and the value of the hole drift mobility in the TBA glass was found to be $1.5x10^{-4}$ $cm^2V^{-1}s^{-1}$ at an electric field of $2.0x10^5$ $Vcm^{-1}$ at 293 K. *o*- and *p*-TTA showed higher room-temperature mobilities than that of TBA.

The room-temperature mobilities of *o*- and *p*-TTA were almost the same, being more than one order of magnitude higher than that of *m*-TTA as shown in Table 3-2. In

terms of eqn. 3-11, smaller $E_0$ in *o*-TTA and *p*-TTA is mainly responsible for the higher mobility than that in *m*-TTA. That is, the molecular structure exerts an influence on charge transport through the energetic factor in eqn. 3-11. The parameters, $\mu_0$ and $T_0$, also lower the mobility in *m*-TTA, but it is difficult to discuss the relation between $\mu_0$ and $T_0$, and molecular structure because $\mu_0$ and $T_0$ have no physical meaning.

In terms eqn. 3-11, the difference in the $\mu_h$ of these materials is mainly attributed to the difference in the diagonal disorder, $\sigma$. In the disorder formalism, the $\sigma$ value is determined by three dominant contributions;

$$\sigma = \left(\sigma_{rot}^2 + \sigma_{vdW}^2 + \sigma_{dipole}^2\right)^{1/2} \qquad (3\text{-}12)$$

where, $\sigma_{rot}$ is intramolecular contribution arising from variations of molecular geometry, $\sigma_{vdW}$ van der Waals contribution arising from variations of van der Waals interaction, $\sigma_{dipole}$ dipolar contribution arising from variations of the charge-dipole interaction.

Since *o*-, *m*-, and *p*-TTA do not have polar substituents, the difference in $\sigma_{dipole}$ among these materials can be neglected. The $\sigma_{vdW}$ value can be estimated from the polarizability ($\alpha$), which can be calculated from the eqn. 3-13;

$$\alpha = \frac{3}{4\pi A}\frac{n^2-1}{n^2+2}\frac{M}{d} \qquad (3\text{-}13)$$

where A is the Avogadro's number, M the molecular weight, d the density, and n the refractive index. Since the polarizabilities of *o*-, *m*-, and *p*-TTA are almost the same (96, 97, and 102 $Å^3$, respectively), the difference in $\sigma_{vdW}$ can be neglected. Therefore, the difference in $\sigma_{rot}$ values of *o*-, *m*-, and *p*-TTA is attributed to the difference in the $\sigma$ values of these materials. In the case of *o*-TTA, there is so large steric constrain that the outside biphenyl moieties cannot rotate. This is thought to be responsible for the small $\sigma$ value of *o*-TTA. In the case of *p*-TTA, the steric constrain is small and the outside biphenyl moieties can rotate easily, but the variations of molecular geometry is small because three phenyl groups in the terphenyl moieties are on the straight line. As compared with *o*- and *p*-TTA, the steric constrain in *m*-TTA is relatively small and the

variations of molecular geometry is large. This is thought to be responsible for the large $\sigma$ value of *m*-TTA.

Negative electric-field dependence for a *o*-TTA molecular glass

The drift mobility of charge carriers generally increases with increasing electric field, following the relation $\exp(SE^{1/2})$ as shown in eqn. 3-7 and 3-11. The negative electric-field dependence of charge-carrier drift mobility has also been observed for several molecularly-doped polymer systems at low concentrations.[51,77,86–90] The phenomenon of negative electric-field dependence has been explained in terms of the disorder formalism as arising due to the presence of the off-diagonal disorder.[51,87–90]

Eqn. 3-11 predicts that the slope of the plots of ln $\mu$ *vs.* $E^{1/2}$ is proportional to $C(\hat{\sigma}^2-\Sigma^2)$ and that both the magnitude and the sign of the electric-field dependence are determined by the balance between the two disorder parameters, diagonal ($\sigma$) and off-diagonal ($\Sigma$) disorders. When $\hat{\sigma}^2$ becomes smaller than $\Sigma^2$, the slope of the electric-field dependence of the charge-carrier mobility should become negative.

Figure 3-17 shows the electric-field dependencies of the hole drift mobilities of the *o*-TTA glass at various temperatures. The slope of the electric-field dependence decreased with increasing temperature and became negative at temperatures above 285 K.

The slope S in Figure 3-17 can be described as eqn. 3-14. Figure 3-18 shows the plots of the slope S *vs.* T. The value S became negative above 285 K, showing a negative electric-field dependence of the hole drift mobility.

$$S = \partial \ln(\mu/\mu_0)/\partial E^{1/2} = C(\hat{\sigma}^2-\Sigma^2) \qquad (3\text{-}14)$$

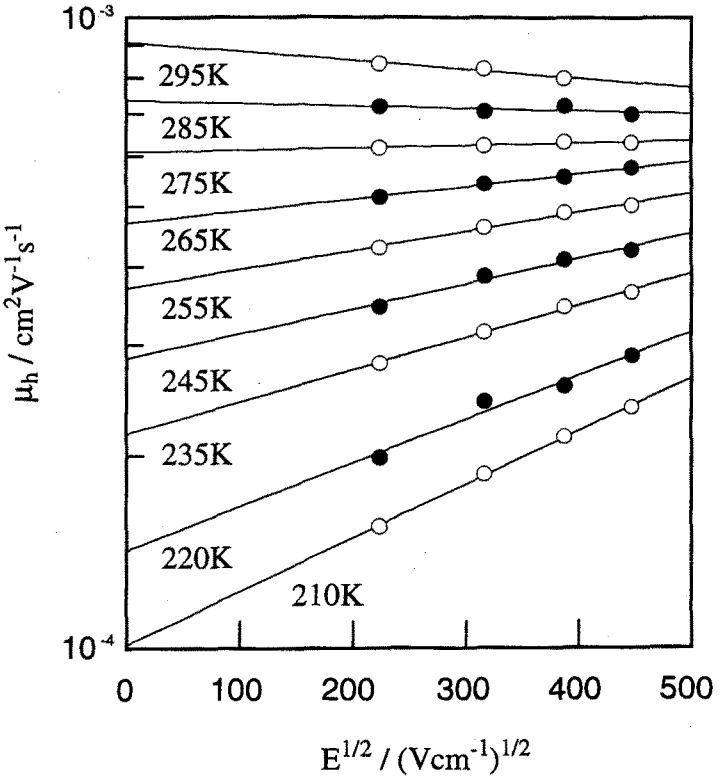


**Figure 3-17** Electric-field dependencies of hole drift mobility for a *o*-TTA glass at different temperatures.

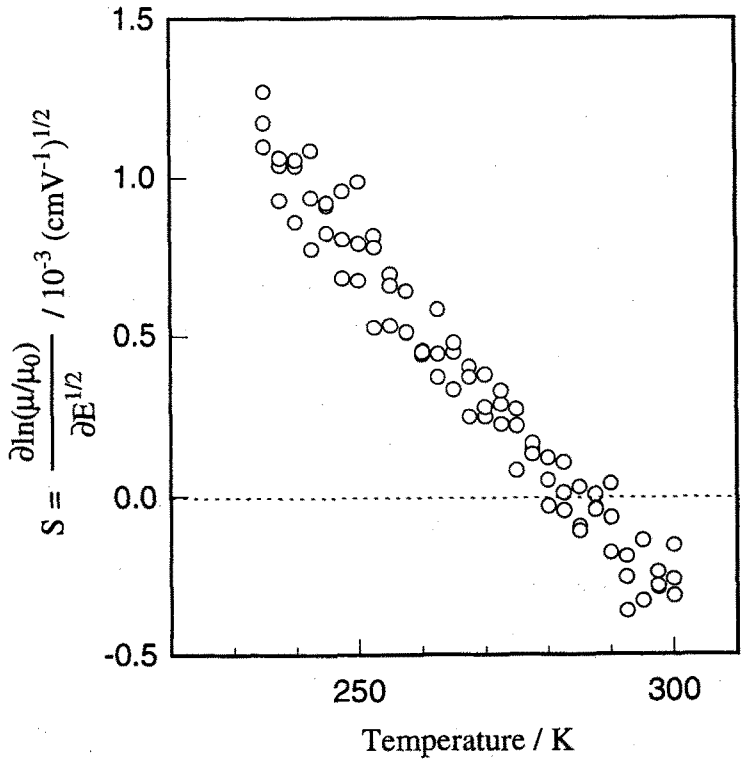


**Figure 3-18** Plots of S as a function of temperature. Here, $S=\partial \ln(\mu/\mu_0)/\partial E^{1/2}$.

The negative electric-field dependence of charge-carrier drift mobility has been understood as arising due to the presence of the off-diagonal disorder $\Sigma$ caused by the fluctuation of the intermolecular $\pi$-electron overlap. That is, there exist faster detour routes against the electric field due to the presence of the off-diagonal disorder $\Sigma$ and that these routes are gradually impeded with increasing electric field.

The phenomenon of negative electric-field dependence of charge-carrier drift mobility has been observed for the molecularly-doped polymer systems at low concentrations (5~25wt%), where a large off-diagonal disorder $\Sigma$ arises due to the interaction between a matrix polymer and a dopant molecule. The $\Sigma$ and $\sigma$ values for the lightly doped polymer systems which exhibit negative electric-field dependence of drift mobility are *e.g.*, $\sigma$=0.12 eV and $\Sigma$=5.0 for 5'-[4-[bis(4-ethylphenyl)aminophenyl]-N,N,N',N'-tetrakis(4-ethylphenyl)-[1,1':3',1"-terphenyl]-4,4"-diamine doped in polycarbonate at 17wt%,[88] $\sigma$=0.097 eV and $\Sigma$=4.6 for tris(*p*-tolyl)amine doped in polystyrene (PS) at 5 wt%.[90] Large $\Sigma$ values for the above systems are responsible for the negative electric-field dependence.

In the present molecular glass of *o*-TTA, however, the $\Sigma$ value ($\Sigma$=2.4) is smaller compared with those for the reported systems exhibiting negative electric-field dependence. The present negative electric-field dependence of the hole drift mobility observed for the *o*-TTA molecular glass is mainly attributed to a very small value of $\sigma$ (0.059 eV). The small variation of molecular geometry of *o*-TTA due to a large steric constrain of the *o*-terphenyl moiety is responsible for the small $\sigma$ value.

## 3-4 Conclusion

Charge transport in the molecular glass of TTPA and in the molecular glasses of *o*-, *m*-, and *p*-TTA was studied. The correlation between the charge-transport properties and the molecular structure was discussed.

It was found that the TTPA glass exhibits a high hole drift mobility approaching to $10^{-3}$ $cm^2V^{-1}s^{-1}$. The small activation energy at zero-electric field in terms of eqn. 3-7 and the small diagonal disorder in terms of eqn. 3-11 are mainly responsible for the high hole drift mobility of TTPA. It is expected that TTPA functions as a good charge transport material for use in photoreceptors in electrophotography and for use in organic electroluminescent devices.

*o*- and *p*-TTA glasses were found to exhibit high room-temperature hole drift mobilities of *ca.* $10^{-3}$ $cm^2V^{-1}s^{-1}$, being one order of magnitude higher than that of *m*-TTA molecular glass. This result was mainly attributed to the difference in the energetic factor in terms of both eqn. 3-7 and eqn. 3-11. It was found that the internal rotation exerts a great influence on charge transport of these materials.

We have found for the first time the negative electric-field dependence of hole drift mobility for the molecular glass without a polymer binder and shown that a small diagonal disorder is responsible for this phenomenon in contrast to a large off-diagonal disorder reported for molecularly-doped polymer systems.

# CHAPTER 4

## Application of Molecular Glasses as Functional Materials – Creation of Molecular Resists

### 4-1 Introduction

Microstructure fabrication technology using photolithographic process, which had been applied to printed circuit in the 1940s, is one of the key technologies in semiconductor industry. The minimum feature size in semiconductor devices has been becoming significantly smaller. Nowadays, 64 Mbit dynamic random access memories (DRAM), which require 0.35 μm resolution, have started in commercial production. The next 256 Mbit DRAMs will be fabricated using 0.25 μm resolution. Research work to achieve 180 nm and 150 nm resolutions required for fabrication of 1 Gbit and 4 Gbit DRAMs, which are expected to appear in the 21st century, has also started.

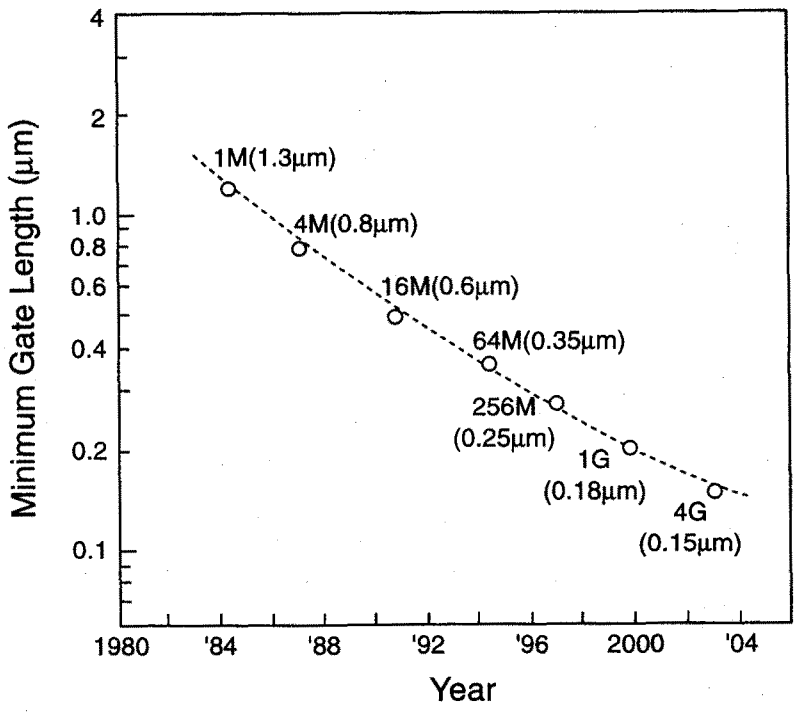


**Figure 4-1** Minimum feature size required for DRAM fabrication.

In order to fabricate the microstructure with such high resolution, development of both the lithographic process including the light source with a shorter wavelength and resist materials are needed. With regard to the light source, development of the photolithographic process using KrF and ArF excimer lasers is now in progress. Furthermore, the lithographic process using electron beam or X-ray has also been investigated. With regard to resist materials, organic polymers have been used owing to their excellent film-forming properties.

One of the well-known positive type photoresists is a mixture of phenol resin (novolac resin) as a base polymer and diazonaphthoquinone as a dissolution inhibitor (Figure 4-2).[91] The diazonaphthoquinone is hydrophobic and inhibits the dissolution of novolac resin into base solution. The diazonaphthoquinone is transformed *via* keto carbene by photosensitized chemical reaction known as Wolff rearrangement. The ketene reacts with water present in the system, and the indene carboxylic acid, which is soluble in base solution, is produced as a final product (Scheme 4.1). The exposed area becomes soluble in base solution and the positive patterns are fabricated. Several types of base resin and dissolution inhibitor have been reported. Other than diazonaphthoquinone, onium salts (Figure 4-3 (a) and (b)), *o*-nitrobenzyl ester (Figure 4-3 (c)), etc., are known as dissolution inhibitors.

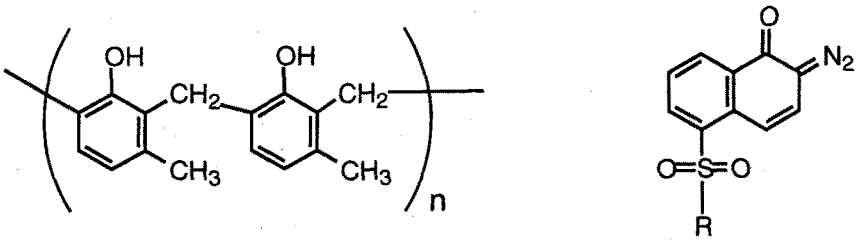


**Figure 4-2** Chemical structure of novolac resin and diazonaphthoquinone.

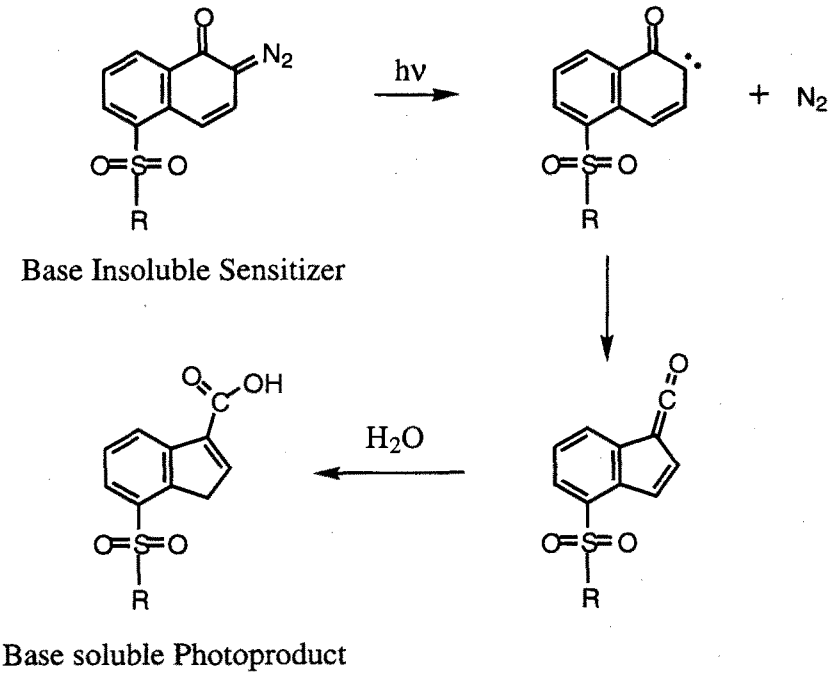


**Scheme 4.1** Photochemical reaction of diazonaphthoquinone.

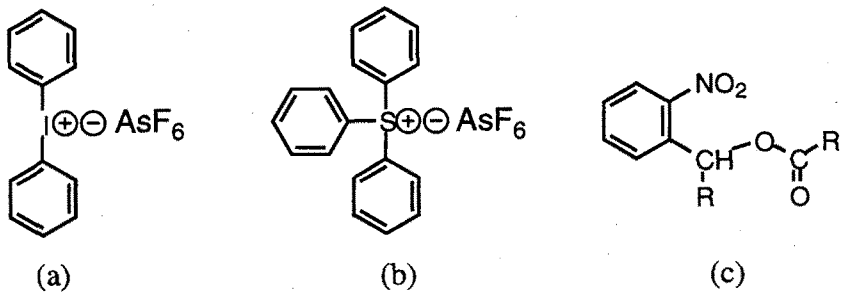


**Figure 4-3** Chemical structure of dissolution inhibitors.

Azide-phenol resin resist system is known as a negative type resist system (Figure 4-4).[92] In this system, 3,3'-diazidediphenylsulfone functions as a cross linker, and the molecular weight of phenol resin increases. This is responsible for the decrease of the solubility of the polymer.

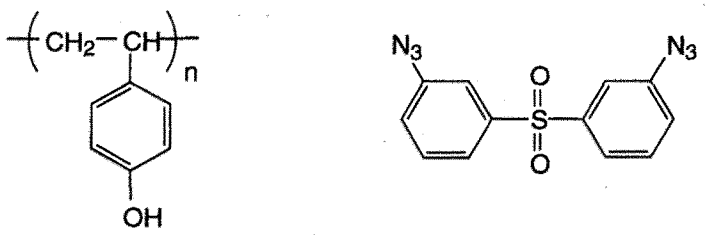

**Figure 4-4** Chemical structure of poly(*p*-vinylphenol) and 3,3'-diazidediphenylsulfone.

Generally the quantum efficiency of photosensitized reaction is less than 1 because one photon absorbed in the resist is used for only one chemical reaction. On the other hand, the quantum efficiency of the chain or catalyzed reaction is more than 1, because the activated species generated by one photon can lead to many chemical reactions. The resist system using such a photochemical reaction with a high quantum efficiency, is a promising system with the high sensitivity, which is called chemical amplification resist. The resist system of poly (*p-tert*-butoxycarbonyloxystyrene) (PBOCST) with onium salt was reported (Figure 4-5).[93] The photogenerated acid by decomposition of onium salt functions as a catalyst of thermal decomposition reaction of PBOCST. Poly(*p*-vinylphenol) is produced as a final product which is soluble in base solution or insoluble in apolar solvents; *i.e.*, this polarity changeable resist functions as both positive and negative type resist. Many other polarity changeable chemical amplification resist systems based on this concept have been developed.

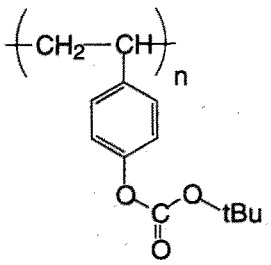

**Figure 4-5** Chemical structure of PBOCST.

The chemical amplification resist using depolymerization reaction is also reported. This type of resist functions as self-developing resist without developer. The resist system using poly(phthaldehyde) (PPA) with onium salt as a photoacid generator is

known as this type of resist system (Scheme 4.2).[94]

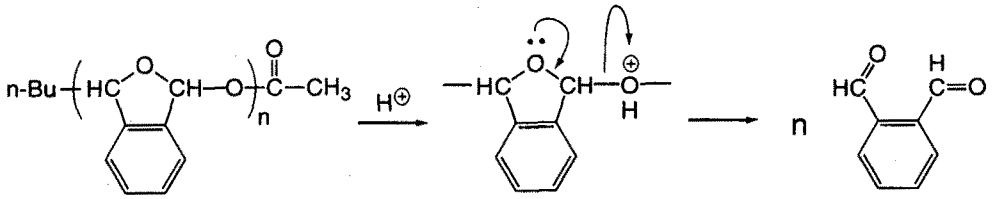

**Scheme 4.2** Depolymerization reaction of PPA in the presence of acid.

The dry developing process using plasma etching instead of wet developing process has received attention because of anisotropic nature of plasma, prevention of swelling and peeling off of the resist film during the wet development process, possibility of high throughput, and prevention of environmental pollution arising from the use and waste of developer. The anti-plasma etching durability is required for the resist used in the dry developing process. Chemical amplification silylating resist is one of the promising resist systems for the dry developing process (Scheme 4.3).[95] The change in polarity means the change in reactivity. The poly(*p*-vinylphenol) generated by decomposition reaction of poly(*p-tert*-butoxycarbonyloxystyrene) can selectively react with silytating agent whereas the poly(*p-tert*-butoxycarbonyloxystyrene) does not react with. In the process of $O_2$ reactive ion etching ($O_2$ RIE), the silyl ether is transformed into $SiO_2$, which prevents the $O_2$ RIE. On the other hand, the nonsilylated part can be etched by $O_2$ RIE, the negative patterns can be obtained.

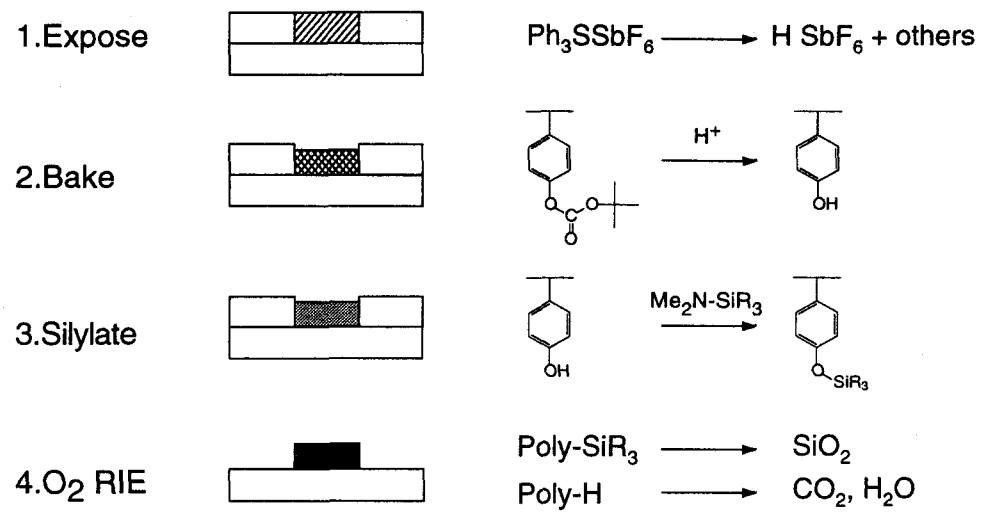


**Scheme 4.3** Dry developing process using chemical amplification silylating resist.

Electron beam and X-ray lithography have been developed (1) for direct writing the lithographic patterns on silicon wafer, and (2) for making masks for projection light irradiation. The materials for masks are a glass substrate on which chrome is vapor deposited (for UV light), a quartz or sapphire substrate on which chrome or aluminum is vapor deposited (for deep UV), a silicon substrate or a polymer film on which gold is vapor deposited (for X-ray). The masks are made by following way; resist film is formed on these substrate by a spin-coat method and irradiated to electron beam. After development of the irradiated film, the vapor deposited films of chrome, aluminum, or gold was etched by wet or dry etching (using plasma or ion). The mask patterns are also fabricated by a lift-off method or electroforming method. After making the mask patterns, the resist film is removed.

When the electron beam or X-ray are irradiated to polymers, cross-linking or cleavage reaction takes place. It can be empirically predictable whether the polymer undergoes cross-linking or cleavage reaction. If the vinyl polymers contain substituents $R^1$ and $R^2$ other than hydrogen, the polymer undergoes cleavage reaction. When both $R^1$ and $R^2$ are halogen atoms, the polymers also undergoes cleavage reaction. If $R^1$ or $R^2$ is hydrogen, cross-linking reaction takes place. Table 4-1 summarizes reactions occurred when vinyl polymers are irradiated to electron beam.

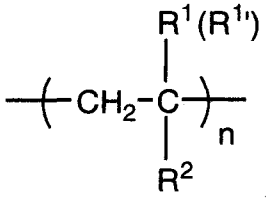

**Table 4-1** Reactions occurred when vinyl polymers are irradiated to electron beam.

| $R^1$ | $R^2$ | cross-linking | $R^{1'}$ | cleavage |
|---|---|---|---|---|
| H | H | polyethylene | | |
| H | H | polymethylene | | |
| H | $CH_3$ | polypropylene | $CH_3$ | poly(isobutylene) |
| H | $C_6H_5$ | polystyrene | $CH_3$ | poly(α-methylstyrene) |
| H | COOH | poly(acrylic acid) | $CH_3$ | poly(methacrylic acid) |
| H | $COOCH_3$ | poly(methylacrylate) | $CH_3$ | poly(methylmethacrylate) |
| H | $CONH_2$ | poly(acrylamide) | $CH_3$ | poly(methacrylamide) |
| H | OR | poly(vinylalkylether) | | |
| H | $COCH_3$ | poly(vinylmethylketone) | $CH_3$ | poly(methylisopropenylketone) |

Methacrylate polymers are known to function as positive type electron beam resists. Poly(methylmethacrylate) (PMMA), [96-98] poly(butylmethacrylate), poly(methyl-methacrylate-*co*-methacrylic acid), poly(methymethacrylate-co-isobutylene),[99] are known. Scheme 4.4 shows the decomposition mechanism of PMMA on exposure to electron beam or X-ray irradiation. At the first stage, the decomposition reactions occur in the side chains by irradiation. Next, carbon monoxide is eliminated and the stable tertiary radical is formed in the main chain. The β-scission takes place and the tertiary radical stabilized by acyl group is formed. The decrease of molecular weight by decomposition reaction in the main chain is the origin of the increase of the solubility of the molecule, thus the PMMA functions as a positive type resist. The sensitivity of PMMA resist film is not high (2 ~$5x10^{-5}$ $Ccm^{-2}$). However, PMMA is one of the resists with high resolution capability and excellent film forming property.

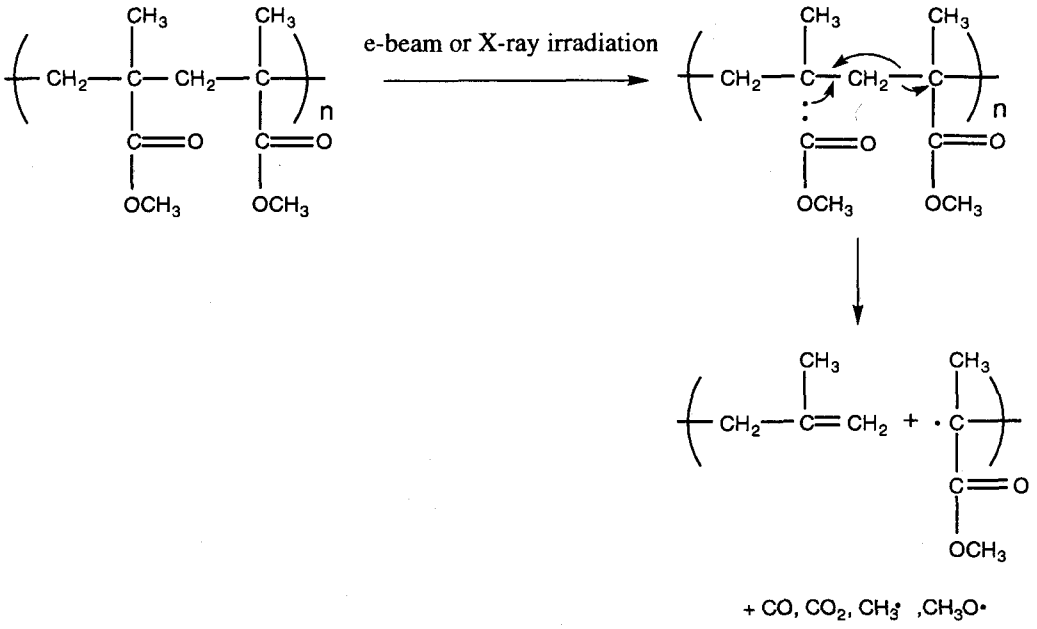


**Scheme 4.4** Decomposition mechanism of PMMA by electron beam or X-ray irradiation.

Other than the methacrylate polymers, polymers containing methyl group at α-position function as positive type electron beam resists. Poly(α-methylstyrene), poly(isobutylene), poly(methylisopropenylketone)[100] are known. The polyolefins containing C-S bond in the main chain are also known as positive resists with high sensitivity because the bonding energy of C-S bond is relatively small (62 kcal $mol^{-1}$).

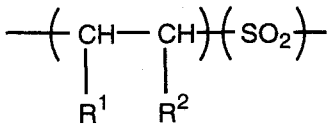

Especially, poly(1-butene sulfone) (PBS) exhibits a high sensitivity (*ca.* $1x10^{-6}$ $Ccm^{-2}$) (Figure 4-6).[101-103]

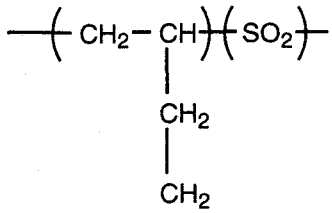

**Figure 4-6** Chemical structure of PBS.

Cross-linkable polymers on exposure to electron beam function as negative type electron beam resists. Poly(acrylamide), poly(vinylchloride),[97] and poly(styrene) are known. Polymers containing the unsaturated double bonds such as polybutadiene also function as negative type electron beam resists.

The polymers containing the epoxy groups are known as negative electron beam resists with higher sensitivity than that of unsaturated polymers. For example, poly glycidyl methacrylate (PGMA) exhibits a high sensitivity ($1x10^{-7}$ ~ $10^{-9}$ $Ccm^{-2}$) (Figure 4-7).[104,105]

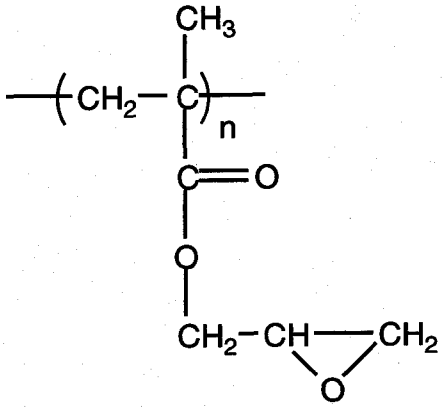

**Figure 4-7** Chemical structure of PGMA.

The resist systems described above are based on the polymers. One of the factors determining the resolution limit of the lithographic pattern is the molecular size of resist materials. For example, in case the polymer chain in the resist is represented as a sphere with a radius proportional to the square root of the chain length, the radius of the sphere of an organic polymer with a degree of polymerization of $10^5$ is roughly calculated to be 10 nm.[106] This means that there is more than 10 % fluctuation in 100 nm lithographic patterns. In order to obtain nanometer-size lithographic patterns, it is desirable to reduce the molecular size of resist materials. Therefore, one of the breakthroughs needed to achieve lithographic patterns of 150 nm or less is the development of low molecular-

weight organic resist materials, which we refer to as "molecular resist". However, little attention has been paid to low molecular-weight organic compounds as candidates for resist materials, since low molecular-weight organic compounds tend to crystallize readily and hence they are not able to form uniform amorphous films. Very recently, an oligomer of a calixarene derivative and a vacuum evaporated film of $C_{60}$ have been reported to function as negative electron-beam resists with high resolution.[107,108]

In our laboratory, we have designed and synthesized several novel families of low molecular-weight organic compounds that readily form stable amorphous glasses, namely molecular glasses which show glass transition usually associated with polymers. In the present study, a new concept of "molecular resist" is proposed and a novel family of resist materials based on this concept, 1,3,5-tris[4-(4-toluenesulfonyloxy)phenyl]benzene (TsOTPB), 1,3,5-tris[4-(*tert*-butoxycarbonyloxymethoxy)phenyl]benzene (BCMTPB) and 4,4',4"-tris(allylsuccinimido)triphenylamine (ASITPA), which function as positive and negative resists with high resolution capability, respectively, on exposure to electron beam is created.

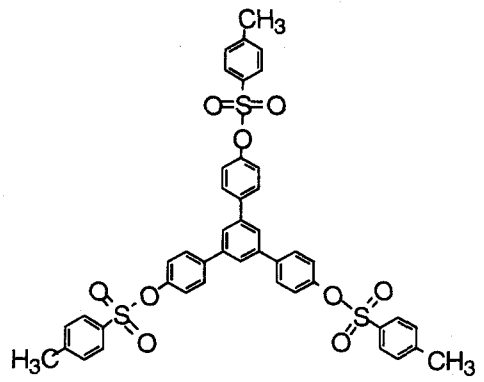

TsOTPB

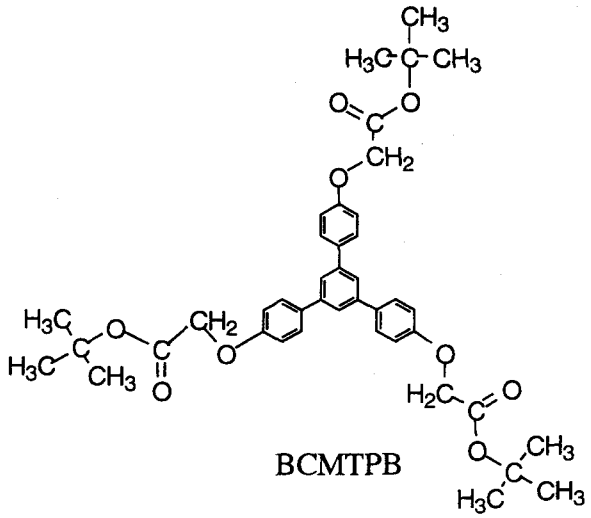

BCMTPB

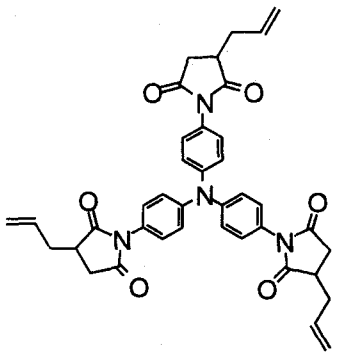

ASITPA

## 4-2 Experimental

Preparation of TsOTPB

The new compound, TsOTPB was synthesized by the condensation reaction of 1,3,5-tris(4-hydroxyphenyl)benzene (5.2g, 15 mmol) with 4-toluenesulfonyl chloride (10.9g, 57 mmol) in pyridine under reflux for 6 h. The resulting mixture was poured into iced water, and the precipitate was collected by filtration. Recrystallization from acetone gave colorless powder (6.5g, 54 %). TsOTPB was identified by the mass spectrometry, various spectroscopy, and elemental analysis. MS: m/z 816 ($M^+$). Calcd. for C45H36O9S3: C, 66.16; H, 4.44; O, 17.63; S, 11.77. Found: C, 65.96; H, 4.37; S, 11.71. $^1$H NMR (400 MHz, solvent: acetone-$d_6$, standard: tetramethylsilane) δ(ppm) =2.47 (9H, s), 7.15 (6H, d), 7.50 (6H, d), 7.79 (6H, d), 7.84 (6H, d), 7.86 (3H, s).

Preparation of BCMTPB

The new compound, BCMTPB was synthesized by the condensation reaction of 1,3,5-tris(4-hydroxyphenyl)benzene (3.5g, 10mmol) with chloroacetic acid *tert*-butyl ester (7.0g, 46 mmol) in tetrahydrofuran in the presence of potassium carbonate anhydrous and 1,4,7,10,13,16-hexaoxacyclooctadecane (18-crown-6). The resulting mixture was extracted by benzene, and dried over sodium sulfate anhydrous. After evaporation of solvent, the residue was chromatographed on silica gel column using benzene as an eluent. Recrystallization from benzene / hexane gave a white needle crystal (2.0g, 28 %). BCMTPB was identified by mass spectrometry, various spectroscopy, and elemental analysis. MS: m/z=696 ($M^+$). Calcd. for C42H48O9: C, 72.39; H, 6.94; O, 20.67. Found: C, 72.25; H, 6.95. $^1$H NMR (400MHz, solvent: acetone-$d_6$, standard: tetramethylsilane) δ(ppm)=7.78 (6H, d), 7.77 (3H, s), 7.05 (6H, d), 4.67 (6H,s), 1.48 (27H, m).

Preparation of ASITPA

The new compound, ASITPA was synthesized by the condensation reaction of tris(4-aminophenyl)amine (2g, 7mmol) with allylsuccinic anhydride (4g, 29mmol) in mesitylene at 130 ℃ for 20 h under nitrogen atmosphere. The resulting mixture was washed by aqueous sodium hydrogencarbonate and water. After evaporation of solvent, the residue was chromatographed on silica gel column using benzene / acetone as an eluent. Recrystallization from tetrahydrofuran / hexane gave a colorless powder (0.6g, 9 %). ASITPA was identified by mass spectrometry, various spectroscopy, and elemental analysis. MS: m/z=656 ($M^+$). Calcd. for C39H36N4O6: C, 71.33; H, 5.53; N, 8.53; O, 14.62. Found: C, 70.80; H, 5.46; N, 8.45. $^1$H NMR (400MHz, solvent: benzene-$d_6$, standard: tetramethylsilane) δ(ppm)=7.25 (6H, d), 6.98 (6H, d), 5.41 (3H, m), 4.87 (3H, d), 4.81 (3H, dd), 2.22 (3H, m), 2.15 (3H, m), 2.09 (3H, dd), 1.95 (6H, m).

Lithographic Process

Silicon wafer was treated by the hydrogen fluoride to remove the $SiO_2$ layer and then washed by water, acetone and trichloroethylene, and then dried. The resist films of TsOTPB, BCMTPB, and ASITPA with a thickness of *ca.* 0.5 μm were spin coated from a dilute tetrahydrofuran solution onto a silicon wafer, which was pre-treated with hexamethyldisilazane vapor. Prebaking of the silicon wafer coated with the resist film was carried out at 50 ℃ (for TsOTPB and ASITPA) and at 30 ℃ (for BCMTPB) for 10 min. Electron-beam exposure was performed with a focused electron beam using a scanning electron microscopy (SEM), JEOL EBX-5B for 20 keV electron-beam exposure and JEOL JSM-NSF 2D for 50 keV electron-beam exposure. The development was carried out with a mixed solvent of 5 wt% tetramethylammonium hydroxide (TMAH) and isopropyl alcohol (IPA) (1:1) for 5 s for TsOTPB and BCMTPB to remove the films in the exposed area, and with 2-methoxyethyl acetate for 10 s for ASITPA to remove the film in the unexposed area. After the process of development, the remaining film was rinsed with water and then dried.

Molecular weight of the polymer were measured with a Model 600 gel permeation chromatography system (Waters, Ltd.) using tetrahydrofuran as an eluent. The calibration curve was obtained using polystyrene standards.

Apparatus

DSC measurement was made using a Seiko DSC220C. X-Ray diffraction measurement was carried out with a M18XHF-SRA X-ray diffractometer (MAC Science). Polarizing microscopy was performed with an Optiphot X2 (Nikon) microscope, fitted with a TH-600PM hot stage (Linkam) and crossed polarizers. Film thickness was measured using a Nanospec / AFT microarea gauge (NANOMETRICS).

## 4-3 Synthesis of TsOTPB, BCMTPB, and ASITPA

TsOTPB and BCMTPB were successfully prepared by condensation reaction of 1,3,5-tris(4-hydroxyphenyl)benzene with 4-toluenesulfonyl chloride and with chloroacetic acid *tert*-butyl ester, respectively (Scheme 4.5 and Scheme 4.6). ASITPA was successfully synthesized by condensation reaction of 1,3,5-tris(4-aminophenyl)-amine with allylsuccinic anhydride (Scheme 4.7).

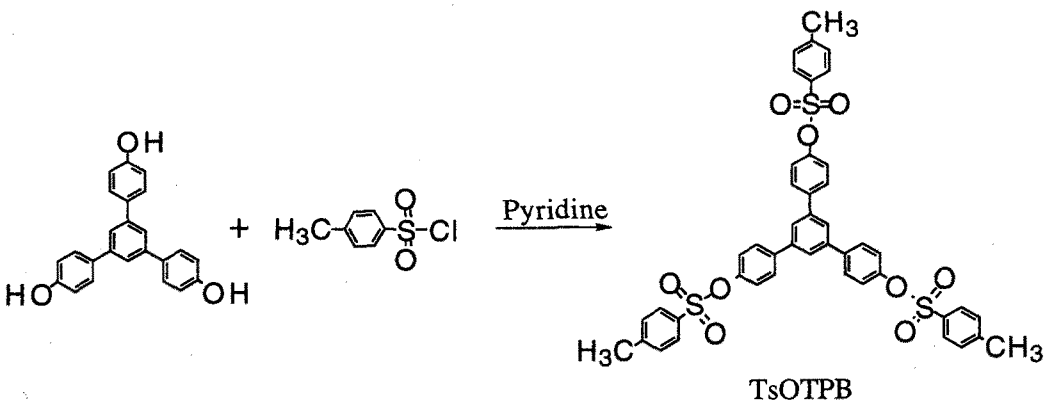


**Scheme 4.5** Synthesis of TsOTPB.

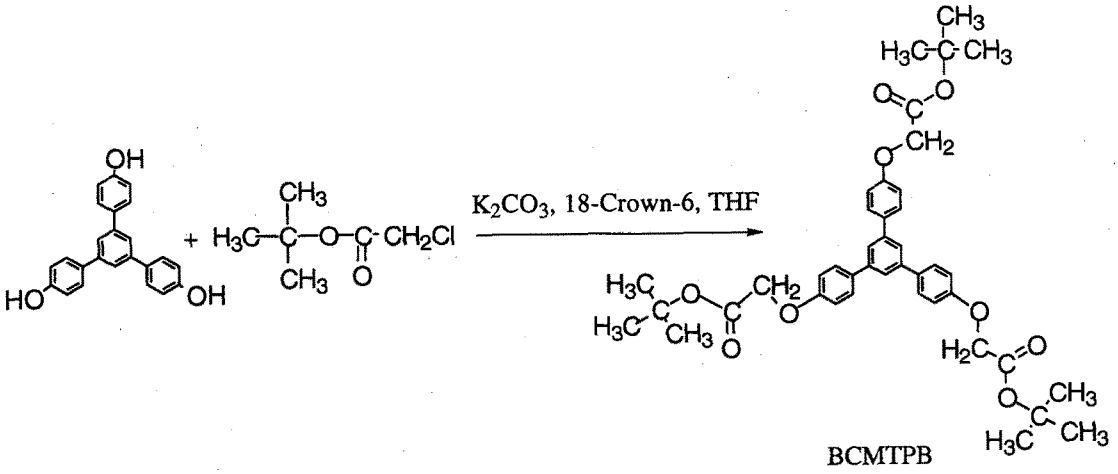


**Scheme 4.6** Synthesis of BCMTPB.

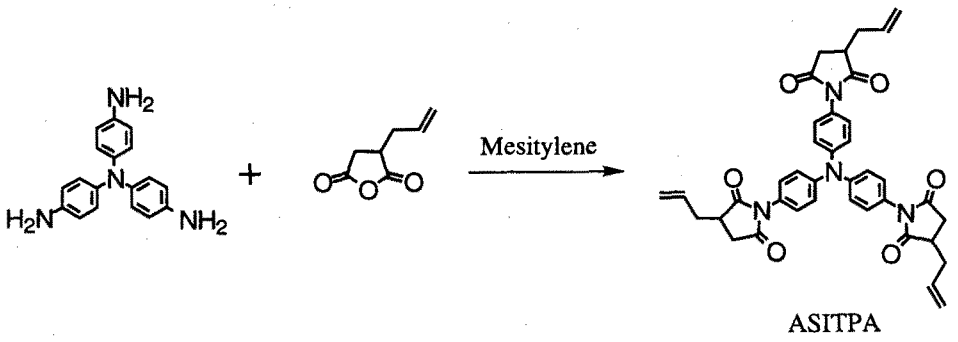


ASITPA

**Scheme 4.7** Synthesis of ASITPA.

## 4-4 Glass-forming Property

The new compounds, TsOTPB, BCMTPB, and ASITPA were found to readily form amorphous glasses when cooled from the melts. Figure 4-8 shows DSC curves of TsOTPB as an example. When the recrystallized sample obtained by recrystallization from acetone was heated, an endothermic peak due to melt is observed at 163 ℃. When the resulting isotropic liquid was cooled on standing in air, it formed an amorphous glassy state *via* a supercooled liquid state. When the amorphous glass sample was again heated, glass transition took place at around 64 ℃. No crystallization behavior was observed on further heating above the glass-transition temperature. The formation of the amorphous glassy state was also evidenced by X-ray diffraction and polarizing microscopy.

Like TsOTPB, BCMTPB and ASITPA were found to form amorphous glasses when cooled from the melts. The glass-transition temperatures of BCMTPB and ASITPA were 34 ℃ and 80 ℃, respectively. TsOTPB, BCMTPB, and ASITPA form uniform amorphous thin films by a spin-coat method.

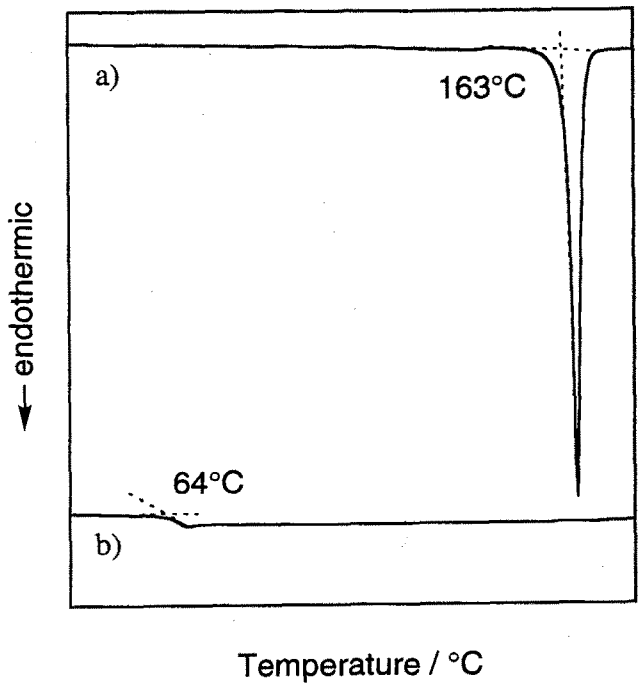


**Figure 4-8** DSC curves of TsOTPB. Heating rate; 5 °Cmin$^{-1}$. a) Crystalline sample obtained by recrystallization from acetone. b) Glass sample obtained by cooling the melt at a cooling rate of 50 °Cmin$^{-1}$.

## 4-5 TsOTPB and BCMTPB as Positive Electron Beam Molecular Resists

The electron-beam irradiated TsOTPB and BCMTPB became soluble in mixed solvent of 5 wt% TMAH / IPA (1:1). Thus, both TsOTPB and BCMTPB function as positive resists. TsOTPB is suggested to undergo cleavage reaction at the sulfur-oxygen bond to generate 4-toluenesulfonic acid and 1,3,5-tris(4-hydroxyphenyl)benzene as the final products. BCMTPB is also suggested to undergo cleavage reaction to generate 2-methylpropene and 1,3,5-tris[4-(carbonylmethoxy)phenyl]benzene as the final products. These are evidenced by the appearance of a O-H band in the FT-IR spectrum of the electron-beam irradiated TsOTPB. It has been reported that some sulfonic acid esters such as 1,2,3-tris(benzenesulfonyloxy)benzene produce the sulfonic acid on photoirradiation or electron-beam irradiation and that they serve as acid generators.[109,110]

Figure 4-9 shows sensitivity curves for TsOTPB and BCMTPB positive resist films,

respectively, on 20 keV electron-beam exposure. The sensitivities were approximately 3 mC $cm^{-2}$ and 1.3 mC $cm^{-2}$ for TsOTPB and BCMTPB, respectively.

Figure 4-10 and Figure 4-11 show SEM images of positive-tone line and space patterns for the TsOTPB and BCMTPB resist films on exposure to 50 keV electron beam at 14 mC $cm^{-2}$. Line patterns of 150 nm could be fabricated for the TsOTPB and BCMTPB positive resist films.

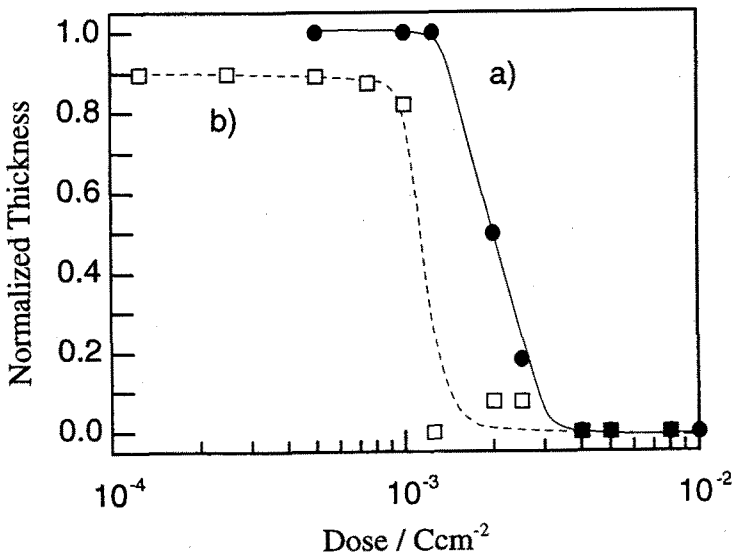


**Figure 4-9** Sensitivity curves for a) TsOTPB and b) BCMTPB on exposure to 20 keV electron beam.

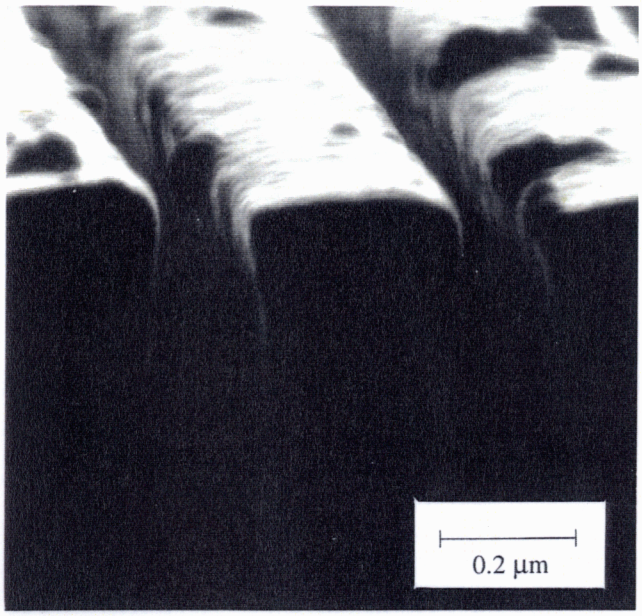


**Figure 4-10** SEM image of positive-tone line and space patterns for the TsOTPB film on exposure to 50 keV electron beam at 14 mC $cm^{-2}$.

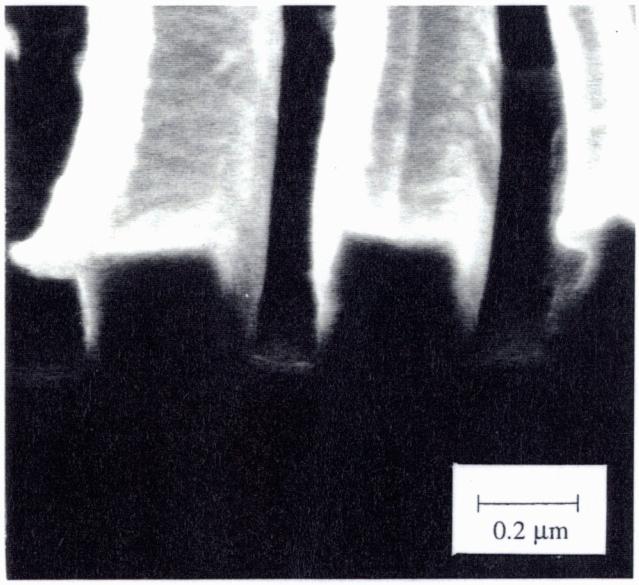


**Figure 4-11** SEM image of positive-tone line and space patterns for the BCMTPB film on exposure to 50 keV electron beam at 14 mC $cm^{-2}$.

## 4-6 ASITPA as a Negative Electron Beam Molecular Resist

The electron-beam irradiated ASITPA became insoluble in 2-methoxyethyl acetate. Thus, ASITPA functions as negative resist. ASITPA, which has three cross-linkable allyl groups, undergoes cross-linking reaction by electron-beam irradiation. The polymers obtained by electron-beam irradiation of ASITPA had a number-average molecular weight of 56,000 and a molecular weight distribution of 1.4, as determined by gel permeation chromatography using polystyrene as a standard.

Figure 4-12 shows sensitivity curve for ASITPA resist film on 20 keV electron-beam exposure. The sensitivity was approximately 3.5 mC $cm^{-2}$ for ASITPA.

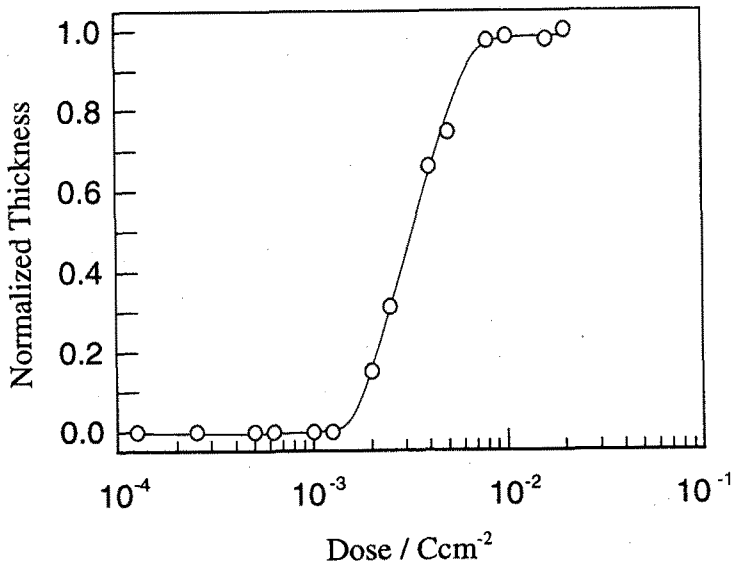


**Figure 4-12** Sensitivity curve for ASITPA resist film on exposure to 20 keV electron beam.

Figure 4-13 shows a SEM image of negative-tone line and space patterns for the ASITPA resist film on exposure to 50 keV electron beam at 12 mC $cm^{-2}$. Line patterns of 70 nm could be fabricated for the ASITPA negative resist film.

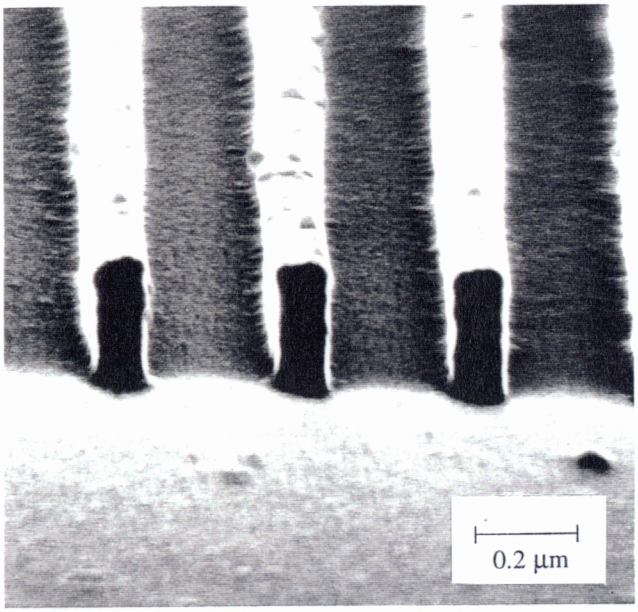


**Figure 4-13** SEM image of negative-tone line and space patterns for the ASITPA resist film on exposure to 50 keV electron beam at 12 mC $cm^{-2}$

## 4-7 Conclusion

We have designed and synthesized a novel family of molecular resist materials, TsOTPB, BCMTPB, and ASITPA, which function as positive and negative resists with high resolution capability, respectively. The TsOTPB, BCMTPB, and ASITPA molecular resists enabled the fabrication of 150 ~ 70 nm line patterns on exposure to electron beam, that is, these molecular resists are capable of fabrication of the DRAMs larger than 4 Gbit which are expected to be appear in 21st century. The present study presents a new concept for future development of molecular resist materials that are expected to be candidates for materials for future nanometer lithography.

# SUMMARY

For the purpose of creation of molecular glasses, novel classes of low molecular-weight organic π-electron systems were designed and synthesized, and their glass-forming properties and morphological changes were studied. Charge transport properties and application of molecular glasses as functional materials were also investigated.

The new compounds synthesized in this study were found to readily form amorphous glasses when cooled from the melts. Two guidelines for creation of molecular glasses were established, *i.e.*, (i) increasing the number of conformers by introduction of an asymmetry moiety or substituents lowers the symmetry of the molecule and hence prevents crystallization, and (ii) the ease of glass formation, glass-transition temperature, and stability of the glassy state are increasing by the introduction of more bulky and heavier substituent.

As a part of our studies of the electronic properties of molecular glasses, charge transport in the glassy state was investigated and the correlation between molecular structure and the charge transport properties was discussed. The internal rotation was found to exert a great influence on charge transport. The negative electric-field dependence of charge carrier drift mobility was found for the first time for the molecular glass.

Finally, as a part of our studies of application of molecular glasses as functional materials, a novel class of low molecular-weight organic resist materials was created. These new resists enabled the fabrication of 150 ~ 70 nm line patterns, which are higher resolution than the line patterns required for fabrication of future 4 G DRAMs (150 nm), on exposure to electron beam. The present study presents a new concept for future development of "molecular resist" that are expected to be candidates for materials for future nanometer lithography.

# References


1 E. A. Silinsh, *Organic Molecular Crystals*, (Springer-Verlag, Berlin, 1980).

2 R. J. Green and D. Turnbull, *J. Phys. Chem.*, **46**, 1243 (1967).

3 Y. Maruyama, T. Iwaki, T. Kajiwara, I. Shirotani, and H. Inokuchi, *Bull. Chem. Soc. Jpn.*, **43**, 1259 (1970).

4 Y. Maruyama and N. Iwasaki, *Chem. Phys. Lett.*, **24**, 26 (1974).

5 Y. Maruyama and T. Yamada, *J. Non-Cryst. Solids*, **28**, 143 (1978).

6 T. Onaka-Ito, and Y. Maruyama, *Mol. Cryst. Liq. Cryst.*, **91**, 187 (1983).

7 H. Nakayama, M. Kawahara, K. Tanabe, K. Ishii, *Mol. Cryst. Liq. Cryst.*, **218**, 183 (1992).

8 K. Ishii, H. Nakayama, K. Tanabe, and M. Kawahara, *Chem. Phys. Lett.*, **198**, 236 (1992).

9 B. Rosenberg, *J. Chem. Phys.*, **31**, 238 (1959).

10 D. J. Plazek and J. H. Magill, *J. Chem. Phys.*, **45**, 3038 (1966).

11 Y. Sano, K. Kato, M. Yokoyama, Y. Shirota, and H. Mikawa, *Mol. Cryst. Liq. Cryst.*, **36**, 137 (1976).

12 Y. Shirota, T. Kobata, and N. Noma, *Chem. Lett.*, 1145 (1989).

13 A. Higuchi, H. Inada, and Y. Shirota, *Adv. Mater.*, *3*, 549 (1991).

14 A. Higuchi and Y. Shirota, *Mol. Cryst. Liq. Cryst.*, **242**, 127 (1994).

15 Y. Kuwabara, H. Ogawa, H. Inada, N. Noma, and Y. Shirota, *Adv. Mater.*, **6**, 677 (1994).

16 D. Okuda, H. Inada and Y. Shirota, *Ann. Meeting of Jpn. Chem. Soc., Preprint*, 635 (1995); submitted for publication in *J. Luminescence*.

17 W. Ishikawa, H. Inada, H. Nakano and Y. Shirota, *Chem. Lett.*, 1731 (1991).

18 W. Ishikawa, H. Inada, H. Nakano and Y. Shirota, *Mol. Cryst. Liq. Cryst.*, **211**, 431 (1992).

19 W. Ishikawa, H. Inada, H. Nakano, and Y. Shirota, *J. Phys. D : Appl. Phys.*, **26**, B94 (1993).

20 E. Ueta, H. Nakano, and Y. Shirota, *Chem. Lett.*, 2397 (1994).

21 W. Ishikawa, K. Noguchi, Y. Kuwabara, and Y. Shirota, *Adv. Mater.*, **5**, 559 (1993).

22 H. Inada and Y. Shirota, *J. Mater. Chem.*, **3**, 319 (1993).

23 Y. Shirota, Y. Kuwabara, H. Inada, T. Wakimoto, H. Nakada, Y. Yonemoto, S. Kawami, and K. Imai, *Appl. Phys. Lett.*, **65**, 807 (1994).

24 H. Inada, Y. Yonemoto, T. Wakimoto, K. Imai, and Y. Shirota, *Mol. Cryst. Liq. Cryst.*, **280**, 331 (1996).

25 A. Higuchi, K. Ohnishi, S. Nomura, H. Inada, and Y. Shirota, *J. Mater. Chem.*, **2**, 1109 (1992).

26 H. Inada, K. Ohnishi, S. Nomura, A. Higuchi, H. Nakano, and Y. Shirota, *J. Mater. Chem.*, **4**, 171 (1994).

27 K. Nishimura, T. Kobata, H. Inada, and Y. Shirota, *J. Mater. Chem.*, **1**, 897 (1991).

28 K. Nishimura, H. Inada, T. Kobata, Y. Matsui, and Y. Shirota, *Mol. Cryst. Liq. Cryst.*, **217**, 235 (1992).

29 S. Nomura, K. Nishimura, and Y. Shirota, *Mol. Cryst. Liq. Cryst.*, **253**, 79 (1994).

30 S. Nomura, K. Nishimura, and Y. Shirota, *Thin Solid Films*, **273**, 27 (1996).

31 Y. Hamada, T. Sano, K. Shibata, and K. Kuroki, *Jpn. J. Appl. Phys.*, **34**, L824 (1995).

32 SAPI91: Fan Hai-Fu (1991). Structure Analysis Program with Intelligent Control, Rigaku Corporation, Tokyo, Japan.

33 P. T. Beurskens; DIRDIF: Direct methods for Difference Structures - an automatic procedure for phase extension and refinement of difference structure factors. Technical Report 1984/1 Crystallography Laboratory, Toernooiveld, 6525 Ed Nijmegen, Netherlands.

34 D. T. Cromer and J. T. Waber, *International Tables for X-Ray Crystallography*, Kynoch Press, Birmingham, England. Vol. IV, p. 71 (1974).

35 TEXSAN - TEXRAY Structure Analysis Package, Molecular ssStructure Corporation (1985).

36 W. C. Hamilton, *Acta Cryst., 12*, 609 (1959).

37 W. S. Sheldrick, W. Becker, and J. Engel, *Acta Cryst.*, **B34**, 3120 (1978).

38 P. W. Codding, *Acta Cryst.*, **C43**, 1394 (1987).

39 L. A. M. Baxter, A. J. Blake, R. O. Gould, G. A. Heath, and T. A. Stephenson, *Acta Cryst.*, **C49**, 1311 (1993).

40 Ng. Ph. Buu-Hois, *J. Chem. Soc.*, 4346 (1952).

41 R. G. Beaman, *J. Polym. Sci.*, **9**, 470 (1952).

42 R. F. Boyer, *J. Appl. Phys.*, **25**, 825 (1954).

43 M. A. Abkowitz, M. Stolka, and M. Morgan, *J. Appl. Phys.*, **52**, 3453 (1981).

44 H. Bässler, G. Schönherr, M. Abkowitz, and D. M. Pai, *Phys. Rev. B* , **26**, 3105 (1982).

45 M. Stolka, J. F. Yanus, and D. M. Pai, *J. Phys. Chem.*, **88**, 4707 (1984).

46 S. J. Santos Lemus and J. Hirsch, *Philos. Mag.*, **B53**, 25 (1986).

47 L. B. Schein, A. Rosenberg, and S. L. Rice, *J. Appl. Phys.*, **60**, 4287 (1986).

48 L. B. Schein and J. X. Mack, *Chem. Phys. Lett.*, **149**, 109 (1988).

49 J. X. Mack, L. B. Schein, and A. Peled, *Phys. Rev. B*, **39**, 7500 (1989).

50 L. B. Schein, D. Glatz, and J. C. Scott, *Phys. Rev., Lett.*, **65**, 472 (1990).

51 A. Peled, L. B. Schein, and D. Glatz, *Phys. Rev. B* , **41**, 10835 (1990).

52 P. M. Borsenberger, *J. Appl. Phys.*, **68**, 6263 (1990).

53 H. -J. Yuh and D. M. Pai, *Philos. Mag. Lett.*, **62**, 61 (1990).

54 P. M. Borsenberger, T. M. Kung, and W. B. Vreeland, *J. Appl. Phys.*, **68**, 4100 (1990).

55 T. Kitamura and M. Yokoyama, *J. Appl. Phys.*, **71**, 300 (1992).

56 Y. Kanemitsu, H. Funada, and Y. Matsumoto, *J. Appl. Phys.*, **71**, 300 (1992).

57 M. Sugiuchi and H. Nishizawa, *J. Imag. Sci. Technol.*, **37**, 245 (1993).

58 P. M. Borsenberger, E. H. Magin, M. Van der Auweraer, and F. C. DeSchryver, *Phys. Status Solidi A*, **140**, 9 (1993).

59 H. Bässler, *Adv. Mater.*, **5**, 662 (1993).

60 H. Scher and E. W. Montroll, *Phys. Rev. B*, **12**, 2445 (1975).

61 G. Pfister and C. H. Griffiths, *Phys. Rev. Lett.*, **40**, 659 (1978).

62 W. D. Gill, *J. Appl. Phys.*, **43**, 5033 (1972).

63 D. Emin, in P. G. Le Comber and J. Mort (Eds.), *Electronic and Structural Properties of Amorphous Semiconductors*, Academic Press, New York, 1973, Chapter 7.

64 H. Bässler, *Phys. Status Solidi B*, **107**, 9 (1981).

65 G. Schönherr, H. Bässler, and M. Silver, *Philos. Mag.*, **B44**, 47 (1981).

66 G. Schönherr, H. Bässler, and M. Silver, *Philos. Mag.*, **B44**, 369 (1981).

67 H. Bässler, *Philos. Mag.*, **B50**, 347 (1984).

68 L. Pautmeier, R. Richert, and H. Bässler, *Philos. Mag. Lett.*, **59**, 325 (1989).

69 L. Pautmeier, R. Richert, and H. Bässler, *Synth. Met.*, **37**, 271 (1990).

70 L. Pautmeier, R. Richert, and H. Bässler, *Philos. Mag.*, **B63**, 587 (1991).

71 H. Bässler, *Phys. Status Solidi B*, **175**, 15 (1993).

72 P. M. Borsenberger and H. Bässler, *J. Imag. Sci.*, **35**, 79 (1991).

73 E. H. Magin and P. M. Borsenberger, *J. Appl. Phys.*, **73**, 787 (1993).

74 Y. Yamaguchi, H. Tanaka, and M. Yokoyama, *J. Chem. Soc. Chem. Commun.*, 222 (1990).

75 Y. Yamaguchi, T. Fugiyama, and M. Yokoyama, *Can. J. Chem.*, **69**, 759 (1991).

76 T. Sasakawa, T. Ikeda and S. Tazuke, *J. Appl. Phys.*, **65**, 2750 (1989).

77 H.-Y. Yuh and D. M. Pai, *Mol. Cryst. Liq. Cryst.*, **183**, 217 (1990).

78 P. M. Borsenberger, *J. Appl. Phys.*, **68**, 5188 (1990).

79 P. M. Borsenberger and H. Bässler, *J. Chem. Phys.*, **95**, 5327 (1991).

80 P. M. Borsenberger and L. J. Rossi, *J. Chem. Phys.*, **96**, 2390 (1992).

81 P. M. Borsenberger, E. H. Magin, and J. J. Fitzgerald, *J. Phys. Chem.*, **97**, 8250 (1993).

82 P. M. Borsenberger and H. Bässler, *Phys. Status. Solidi B*, **170**, 291 (1992).

83 P. M. Borsenberger and J. J. Fitzgerald, *J. Phys. Chem.*, **97**, 4815 (1993).

84 M. Van der Auweraer, F. C. DeSchryver, P. M. Borsenberger, and J. J. Fitzgerald, *J. Phys. Chem.*, **97**, 8808 (1993).

85 P. M. Borsenberger, L. T. Pautmeier, and H. Bässler, *Phys. Rev. B*, **46**, 12145 (1992).

86 A. Peled and L. B. Schein, *Chem. Phys. Lett.*, **153**, 422 (1988).

87 P. M. Borsenberger, *J. Appl. Phys.*, **68**, 5682 (1990).

88 N. Novo, M. Van der Auweraer, F. C. De Schryver, P. Borsenberger, and H. Bässler, *Phys. Status Solidi B*, **177**, 223 (1993).

89 R. H. Young and N. G. Rule, *Phys. Rev. Lett.*, **72**, 388 (1994).

90 R. H. Young, J. A. Sinicropi, and J. J. Fitzgerald, *J. Phys. Chem.*, **99**, 9497 (1995).

91 W. S. DeForest, "*Photoresist Materials and Processes*", McGraw Hill, NewYork (1975).

92 T. Iwayanagi, T. Kohashi, S. Nonogaki, T. Matsuzawa, K. Douta, and H. Yanazawa, *IEEE Trans. Electron Devices*, **ED-28**, 1306 (1981).

93 C. G. Willson, H. Itoh, J. M. J. Fréchet, T. G. Tessier, and F. M. Houlihan, *J. Electrochem. Soc.*, **133**, 181 (1986).

94 H. Itoh and C. G. Willson, *Polym. Eng. Sci.*, **23**, 1012 (1983).

95 S. A. MacDonald, H. Schlosser, H. Ito, N. J. Clecak, and C. G. Willson, *Chem. Mater.*, **3**, 435 (1991).

96 M. Hatzakis, *J. Electrochem. Soc.*, **116**, 1033 (1969).

97 H. Y. Ku and L. C. Scala, *J. Electrochem. Soc.*, **116**, 980 (1969).

98 A. Harris, *J. Electrochem. Soc.*, **120**, 270 (1973).

99 E. Gipstein, W. Moreau, and O. Need, *J. Electrochem. Soc.*, **123**, 1105 (1976).

100 A. W. Levin, M. Kaplan, and E. S. Poliniak, *Polym. Eng. Sci.*, **121**, 1620 (1974).

101 L. F. Thompson and M. J. Bowden, *J. Electrochem. Soc.*, **120**, 1722 (1973).

102 M. J. Bowden and L. F. Thompson, *J. Appl. Polym. Sci.*, **17**, 3211 (1973).

103 M. J. Bowden, L. F. Thompson, and J. P. Ballantyne, *J. Vac. Sci. Technol.*, **12**, 1294 (1975).

104 T. Hirai, Y. Hatano, and S. Nonogaki, *J. Electrochem. Soc.*, **118**, 669 (1971).

105 L. F. Thompson, F. D. Feit, and R. D. Heidenreich, *Polym. Eng. Sci.*, **14**, 529 (1974).

106 B. H. Zimm and W. H. Stockmayer, *J. Chem. Phys.*, **17**, 1301 (1949).

107 J. Fujita, Y. Ohnishi, Y. Ochiai, and S. Matsui, *Appl. Phys. Lett.*, **68**, 1297 (1996).

108 T. Tada and T. Kanayama, *Jpn. J. Appl. Phys.*, **35**, L63 (1996).

109 L. Schlegel, T. Ueno, H. Shiraishi, N. Hayashi, and T. Iwayanagi, *Chem. Mater.*, **2**, 299 (1990).

110 H. Shiraishi, N. Hayashi, T. Ueno, T. Sakamizu, and F. Murai, *J. Vac. Sci. Technol. B*, **9**, 3343 (1991).

# LIST OF PUBLICATION

1. Striking Effects of Halogen Substituents on the Glass-forming Properties, Glass-transition Temperatures, and Stabilities of the Glassy State of a New Family of Amorphous Molecular Materials, 1,3,5-Tris(4-halogenophenylphenylamino)benzenes
   Hiroshi Kageyama, Koji Itano, Wataru Ishikawa, and Yasuhiko Shirota
   *J. Mater. Chem.*, **6**, 675 (1996).

2. 1,3,5-Tris[4-(*tert*-butoxycarbonylmethoxy)phenyl]benzene as a Novel Electron-beam Positive Resist for Nanometer Lithography
   Motoko Yoshiiwa, Hiroshi Kageyama, Fujio Wakaya, Mikio Takai, Kenji Gamo, and Yasuhiko Shirota
   *J. Photopolym. Sci. Technol.*, **9**, 57 (1996).

3. Novel Class of Low Molecular-weight Organic Resists for Nanometer Lithography
   Motoko Yoshiiwa, Hiroshi Kageyama, Yasuhiko Shirota, Fujio Wakaya, Kenji Gamo, and Mikio Takai
   *Appl. Phys. Lett.*, **69**, 2605 (1996).

4. Photo- and Electro-active Amorphous Molecular Material: Morphology, Structures, and Hole Transport Properties of Tris[4-(2-thienyl)phenyl]amine
   Jun-ichi Sakai, Hiroshi Kageyama, Satoyuki Nomura, Hideyuki Nakano, and Yasuhiko Shirota
   *Mol. Cryst. Liq. Cryst.*, in press.

5. Negative Electric-field Dependence of the Hole Drift Mobility for a Molecular Glass
   Hiroshi Kageyama, Katsuhei Ohnishi, Satoyuki Nomura, and Yasuhiko Shirota
   in preparation.

6. A Novel Family of Amorphous Molecular Materials: Synthesis and Glass-forming Properties of 1,3,5-Tris(halogenophenylphenylamino)benzenes

Hiroshi Kageyama, Koji Itano, Wataru Ishikawa, and Yasuhiko Shirota

in preparation.

7. Charge Transport in the Glassy State of a Novel Class of Amorphous Molecular Materials, Tri(terphenyl-4-yl)amines

Hiroshi Kageyama, Katsuhei Ohnishi, Satoyuki Nomura, and Yasuhiko Shirota

in preparation.

# ACKNOWLEDGMENTS

The work of this thesis was carried out under the guidance of Professor Yasuhiko Shirota at Graduate School of Engineering, Osaka University.

I am grateful to Professor Yasuhiko Shirota for his invaluable guidance and encouragement throughout this work.

I am thankful to Mr. Wataru Ishikawa, Mr. Katsuhei Ohnishi, Mr. Satoyuki Nomura, Mr. Koji Itano, Mr. Jun-ichi Sakai, and Miss Motoko Yoshiiwa for their collaborations.

I am grateful to Dr. Naoki Noma and Dr. Hideyuki Nakano for their advice and helps.

I would like to thank Professor Ginya Adachi and his coworkers (Faculty of Engineering, Osaka University) for allowing the use of X-ray diffraction apparatus, Professor Kenji Gamo and his coworkers (Faculty of Engineering Science, Osaka University) for use of Scanning Electron Microscope, and all members of the analytical center (Faculty of Engineering, Osaka University) for their helps.

I wish to thank all the members of Shirota Laboratory for their encouragement and helps.

Finally, I am very thankful to my parents, brother and his wife for their understanding and support.

Hiroshi Kageyama.

HIROSHI KAGEYAMA